4-20-2010

ATOMIC-FORCE-MICROSCOPE INDENTATION OF ALVEOLAR EPITHELIAL TYPE II CELLS

Catherine Eileen Cozad

To the University Council:

The Thesis Committee for Catherine Eileen Cozad certifies that this is the approved version of the following thesis:

ATOMIC-FORCE-MICROSCOPE INDENTATION OF ALVEOLAR EPITHELIAL TYPE II CELLS

_____
Esra Roan, Ph.D., Major Professor

_____
Eugene C. Eckstein, Ph.D.

_____
Christopher M. Waters, Ph.D.

Accepted for the Graduate Council:

_____
Karen D. Weddle-West, Ph.D.

Vice Provost for Graduate Programs

STATEMENT OF PERMISSION TO USE

In presenting this thesis in partial fulfillment of the requirements for a Master's degree at The University of Memphis, I agree that the Library shall make it available to borrowers under rules of the Library. Brief quotations from this thesis are allowable without special permission, provided that accurate acknowledgement of the source is made.

Permission for extensive quotation from or reproduction of this thesis may be granted by my major professor, or in her absence, by the Head of Interlibrary Services when, in the opinion of either, the proposed use of the material is for scholarly purposes. Any copying or use of the material in this thesis for financial gain shall not be allowed without my written permission.

Signature_____

Date_____

ATOMIC-FORCE-MICROSCOPE INDENTATION OF ALVEOLAR EPITHELIAL TYPE II CELLS

by

Catherine Eileen Cozad

A Thesis

Submitted in Partial Fulfillment of the

Requirements for the Degree of

Master of Science

Major: Biomedical Engineering

The University of Memphis

May 2010

Dedication

Acknowledgements

I would like to acknowledge Christopher M. Waters and his group including Lynn Crosby at the University of Tennessee Health Sciences Center for their isolating ATII cells and troubleshooting cell culture problems; Asylum Research for their helping me to learn fluid imaging; Heather Doty and Jidong Guo for their help teaching me how to image in air; Alison Cozad for her help in creating my MATLAB program; Eugene Eckstein for his help with the preparation of my thesis; my family for their support and patience; and my guiding voice, my advisor Esra Roan. Thanks to all!

Abstract

Cozad, Catherine Eileen. M.S. The University of Memphis. May 2010. Atomic-Force-Microscope Indentation of Alveolar Epithelial Type II Cells. Major Professor: Esra Roan, Ph.D.

Primary rat alveolar epithelial type II (ATII) cells dedifferentiate over time in culture into alveolar epithelial type I (ATI) cells. The mechanical characteristics of ATII cells measured as elastic modulus (E) could be time dependent in culture. An atomic force microscope was used to perform force indentation (F-δ) on the ATII cells, using pyramidal cantilevers with spring constant of 0.03 ± 0.01 N/m. Seven isolations of ATII cells were cultured; square regions in confluent cultures were studied by indentation on a one micrometer grid and estimated to touch 3-6 cells. E values were determined from F-δ curves. Some maps of E had indicated regions of high and low values, presumably reflecting regions with and without nucleus. Median E value was 5.93 (Day 2) and 8.37 kPa (Day 3); significant difference was determined by a non-parametric test, $p \leq 0.001$, indicating that mechanical properties of ATII cells could exhibit time dependence.

Table of Contents

List of Figures

List of Abbreviations

AFM:	Atomic Force Microscope
ANOVA:	Analysis Of Variance
ATI:	Alveolar epithelial Type I
ATII:	Alveolar epithelial Type II
d2, d3, d4:	Day 2, Day 3, Day 4
DMEM:	Dulbecco's Modified Eagle Medium
E:	Elastic Modulus
F-δ:	Force Indentation
FBS:	Fetal Bovine Serum
G:	Shear Modulus
Iso:	Isolation
LVDT:	Linear Variable Differential Transformer
RLF:	Rat Lung Fibroblast
UM:	University of Memphis
UTHSC:	University of Tennessee Health and Science Center

Chapter 1: Introduction

The alveolus is the site for gas exchange within the lung. Alveolar epithelial cells cover the surface of the alveolar walls and form a barrier that controls gas exchange. During tidal breathing, the alveolar basement membrane and epithelial cells that line this membrane experience mechanical loading caused by breathing. Alveolar epithelial type II (ATII) cells, progenitors of alveolar epithelial type I (ATI) cells, dedifferentiate into ATI cells during injury, migrate to close gaps due to wounding, and proliferate (Sugahara, Tokumine, Teruya, & Oshiro, 2006). This differentiation has been shown to take place in culture over 3-8 days (Berrios, Schroeder, & Hubmayr, 2001; Dobbs, Williams, & Brandt, 1985;Fuchs et al., 2003). A precise knowledge of the time-point at which the ATII cells become ATI or ATI-like cells in culture can increase the understanding of wound healing in lungs.

Currently, ATI and ATII cells can be distinguished with the use of bio-chemical markers during fluorescent microscopy (Dobbs et al., 1985). Mechanical properties of alveolar epithelial cells could also be an indication of the cell phenotype because they are related to the structure of the underlying cytoskeleton and because cytoplasmic the cytoskeletal constituents of ATI and ATII cells have dissimilarities. For example, surfactant containing, densely-packed lamellar bodies are unique to ATII cells and they are thought to have a relatively higher elastic modulus than the cytoskeleton (Azeloglu, Bhattacharya, & Costa, 2008). Therefore, the underlying *hypothesis* of this thesis is that

the loss of ATII-like features of primary cells in culture could result in altered mechanical characteristics that are measured with atomic force microscopy (AFM) indentation. In order to test the hypothesis, primary cells are isolated from rats and live cells are mechanically characterized at multiple time points in culture. Appropriate non-parametric statistical analyses are carried out to identify significance of findings.

To support the description of the work, a thorough summary of the current literature and mechanical characteristics of respiratory physiology as it pertains to primary ATII cells are presented in Chapter 2: Background and Literature Review. The application of indentation contact mechanics is discussed in Chapter 3: Materials and Methods. The statistical analysis of the results is provided in this thesis, which is discussed in Chapter 4: Results, and Chapter 5: Discussion. The work was concluded in Chapter 6 and future work is found in Chapter 7.

Problem Statement

Mechanical studies have been performed using various techniques to determine the mechanical characteristics of ATII cells and ATI cells but no studies have been completed using force indentation (F-δ) to characterize the ATII cell mechanical properties over time. The aims of this project were 1) to show the gap in literature related to the mechanics of ATII differentiation; 2) to conduct indentation experiments with the use of the atomic force microscope; and 3) to calculate the elastic modulus of ATII cells as a function of time as well as imaging of their topology. The cells are expected to exhibit a dependence on culture time.

Chapter 2: Background and Literature Review

The background and literature review explores the respiratory physiology and mechanics with special focus on ATII cells, the techniques (magnetic twisting cytometry, optical tweezers, magnetic tweezers, micropipette aspiration, microplates, and atomic force microscopy) for characterizing cell mechanical properties, and mechanical theory for analyzing the indentation of the cells.

Respiratory Mechanics

Respiratory Physiology

The mammalian respiratory system is responsible for providing oxygen by inspiration (inhaling), eliminating carbon dioxide by expiration (exhaling), regulating the blood's hydrogen ion concentration, defending against microbes and trapping and dissolving blood clots arising from systemic veins (Widwaimer, Raff, & Strang, 2003). The processes of inspiration and expiration provide mechnical stimuli to the structures and tissues of the respiratory system (Barrett, Barman, Boitano, & Brooks, 2010). The structure of the respiratory system is a complex branching system which begins with the nasal and oral cavities leading to the trachea. The branching bronchi, bronchioles, terminal bronchioles, respiratory bronchioles, and alveolar ducts terminate at the alveolar sacs, which are composed of alveoli.

Alveoli

The alveoli are micro-scale repeating units of the lung that are composed of alveolar basement membrane, epithelial and endothelial cells, air space, and capillaries (Widwaimer et al., 2003). The alveoli add up to a volume of $4.2 \times 10^6 \mu m^3$ (Ochs et al., 2004) and allow an efficient exchange of gaseous molecules between capillaries and alveolar spaces. Gas exchange occurs via diffusion between the alveoli and surrounding capillaries. Therefore, in an average adult human lung, the overall alveolar surface area is very large at 75 m^2 (Pavelka & Roth, 2005) for the 480 million (Ochs et al., 2004) alveoli. An epithelial cell layer of 0.2 to 0.6 μm lines the basement membrane of the alveolus (Widwaimer et al., 2003).

The alveolus is host to several types of cells: alveolar epithelial type I (ATI), alveolar epithelial type II (ATII), and alveolar macrophages. The ATI and ATII cells reside on the alveolar basement membrane (Fehrenbach, 2001), whereas the alveolar macrophages cells move freely across the inner surface of the alveolus on top of the ATI and ATII cells. The alveolar macrophages are responsible for phagocytizing (engulfing) foreign debris (Fels & Cohn, 1986) such as bacteria that enter the alveolus.

ATI Cells

ATI cells are relatively flat with 0.2 μm of thickness and 50 μm of diameter. They cover 93-97% of the alveolar surface (Widwaimer et al., 2003). The ATI cells are not thought to be capable of regeneration (Berthiaume, 1999; Fehrenbach, 2001; Widwaimer et al., 2003). ATI cells allow for gas exchange within the alveolus. ATI

cells have been suggested as the mechanotransducers of the lung by translating mechanical stimuli into bio-chemical signals (Ashino, Ying, Dobbs, & Bhattacharya, 2000; Fehrenbach, 2001).

ATII Cells

ATII cells are located between the ATI cells and have apical microvilli, cell-to-cell junctions, and a cuboidal shape. These geometric traits help distinguish the ATII from the ATI cells (Cheek, Evans, & Crandal, 1989; Fehrenbach, 2001; Fuchs et al., 2003). ATII cells cover 3-5% of the surface of the alveolus. They are considered the workhorses of the alveolus because they are the progenitor cell for ATI cells and because ATII cells produce surfactant (Boitano, Safdar, Welsh, & Koval et al., 2004; Fehrenbach, 2001). Surfactant controls the surface tension of the alveolar air-fluid barrier and inhibits alveolar wall collapse (Fehrenbach, 2001). Specialized organelles within the ATII cell, lamellar bodies, move surfactant outside of the cell by exocytosis to coat the alveolar cell surfaces. The surfactant is comprised of phospholipids and proteins (Griese, 1999; Van Golde, Batenburg, & Robertson, 1994; Fehrenbach, 2001). The surfactant production is unique to ATII cells: labeling for surfactant containing lamellar bodies is one common way in which ATI, and ATII cells are distinguished.

ATII cells are the progenitors for ATI cells (capacity to differentiate into another cell) and they undergo mitosis to re-establish the ATI cells and maintain a functional air-blood barrier in the alveolus. ATII cells typically replace the alveolar epithelium in 4-5

weeks. However, the replacement time is greatly decreased when there is an injury such as hyperoxic alveolar epithelial damage (Fehrenbach, 2001).

Cultured primary ATII cells are shown to lose their ATII characteristics within 3 to 8 days of post-isolation (Berrios et al., 2001; Fuchs et al., 2003). During such a transformation, ATII cells begin to behave more like ATI cells by flattening and losing their ability to produce surfactant, which is termed transdifferentiation or dedifferentiation. (Fuchs et al., 2003). Markers for determining the time at which this dedifferentiation occurs is an important parameter, because it has been suggested that when the primary ATII cells dedifferentiate into ATI cells, they cannot serve as progenitor cells and are not capable of producing surfactant.

There are dedifferentiation markers for ATII cells including staining for the presence of lamellar bodies (Ehrhardt, Kim, & Lehr, 2005), immunohistochemical labeling (Ehrhardt et al., 2005), gene labeling (Dublin et al., 2004) and ATI or ATII specific lectins (binding proteins) (Fehrenbach, 2001). A study of mechanical properties using magentic twisting cytometry (MTC) as a function of dedifferentiation markers has shown that primary Sprague Dawley rat ATII cells increase their apparent stiffness (dynes/cm^2) over days 2 through 9 past isolation. This type of epithelial cell mechanical characterization is relevant, because there are significant mechanical forces generated during breathing that are experienced by the alveoli and the resident cells. The increased understanding of the way in which various alveolar cell types experience these mechanical loads could lead to improved treatment strategies for lung injuries (Desai, Sinclair, Chapman, Hassid, & Waters, 2007; Sinclair, Molthen, Hayworth, Dawson, &

Waters, 2007). Mechanical properties of epithelial cells as a function of culture time are one aspect that is still not well-described and yet is relevant to mechanics of alveolus.

Cell Mechanical Characterization

There are several methods that have been developed for the characterization of the mechanical responses at the cellular and sub-cellular levels. These methods are explored in this section with an emphasis on atomic force microscopy (AFM) indentation and studies that have evaluated the mechanical characteristics of alveolar epithelial cells.

Magnetic Cytometry

Magnetic Twisting Cytometry (MTC) employs magnetic beads [2-9 μm (Spherotech, Lake Forest IL)] that attach to the specific compartments of a cell (Figure 1). With the use of a magnetic field, the beads are torqued and translated. Then, the measured angular rotation and displacements are utilized to characterize the cytoskeletal mechanical properties. Several studies on ATII and A549 cells using MTC have been completed (Laurent et al., 2002) (Fereol et al., 2008) (Stroetz et al., 2001), in which "apparent" elastic modulus or shear modulus is extracted using complex mechanics analyses.

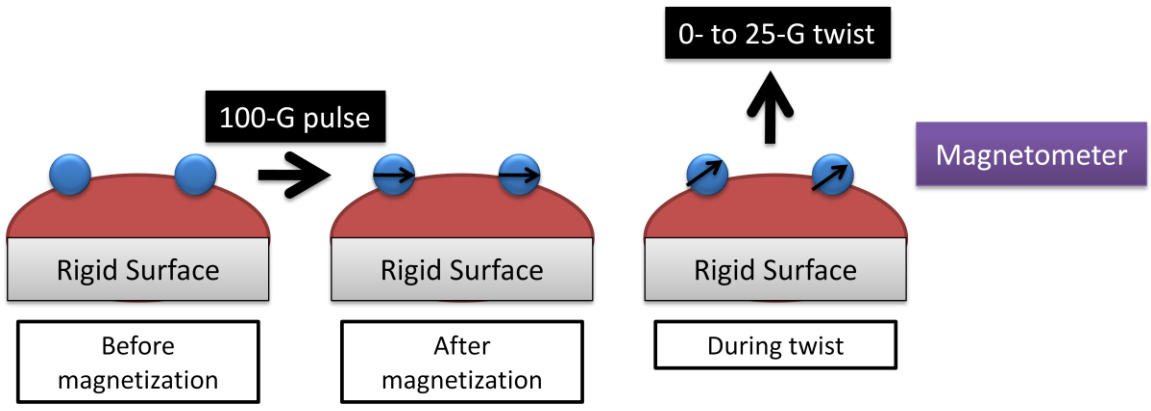

Figure 1. MTC uses magnetic beads to characterize the mechanical response of cells.

The advantage of the MTC is that it allows the mechanical characterization of single cells and intra-cellular components. The disadvantage of MTC is that the measurements are localized, i.e., an overall effective cellular mechanical response is not measured. Moreover, the surface area of the bead-cell interface is not measured resulting in an unknown surface area that is needed for the normalization of the torque or force. The extracted mechanical properties are affected by the unknown surface area as described in full elsewhere (Laurent et al., 2002).

Optical Tweezers

Optical tweezers (OT) measure the cytoskeletal mechanical response of the cell, but apply very small translational forces of 0.1 to 200 pN. This technique focuses a laser beam onto a micro-bead effectively trapping the bead (Figure 2) (Ashkin, Bjorkholm, & Chu, 1986), which is used to apply a force. This force is proportional to the power of the laser and the distance to the bead. Advantages to OT measurements are that this method allows the measurement of mechanical interaction between intra-cellular components

such as lamellar bodies and cytoskeleton. Disadvantages to OT measurements are that the laser introduces thermal loading to the cell, possibly affecting the results. Moreover, OT applies only small loads, and the measurements of the cell are limited to the cytoskeleton similar to the MTC measurements.

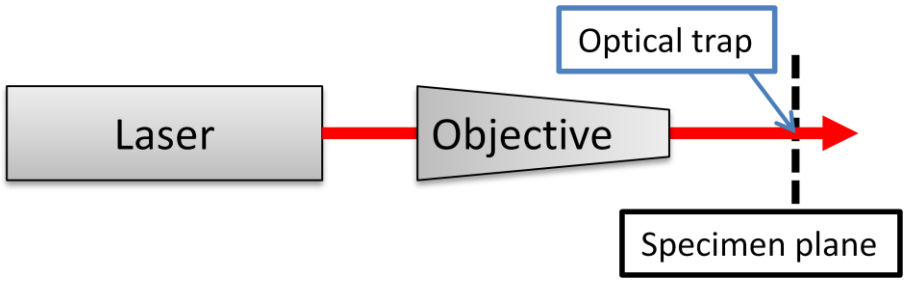

Figure 2. Optical Tweezers; the laser is focused on the specimen plane creating an optical trap for an object or bead within the plane.

Micropipette Aspiration

In the technique of micropipette aspiration, a small pipette contacts the cell plasma membrane to apply a known suction force to pull the cell into the pipette (Figure 3) (Hochmuth, 2000). The micropipette measures the elastic modulus of the cell cytoplasm near the cell surface but not the entire cell. An advantage to the micropipette technique is the low cost of implementation. A disadvantage is that this technique does not measure the elastic modulus of the entire cell and it is difficult to measure adherent flat cells (Zhang, Long, Wu, & Yu, 2002).

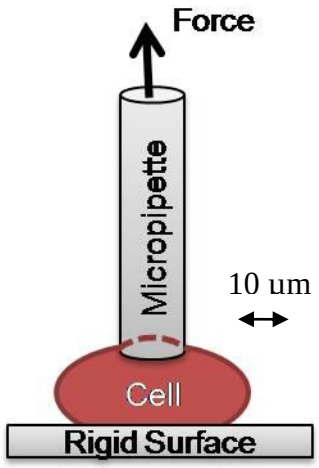

Figure 3. Micropipette aspiration uses a micropipette to apply a force by suction to a cell plasma membrane.

Microplate Loading

The microplates are rectangular glass bars that have flat tips close to the width and 1/10 the length of a cell. The microplates apply a nearly-uniaxial deformation by compressing the cells between a rigid and a flexible microplate (Figure 4), using forces in the range of 1-1000 nN (Thoumine, Ott, Cardoso, & Meister, 1999). The advantages of microplate technique include simple mechanics and the ability to isolate a single cell. The disadvantage of this technique is that the cell must be singled out, i.e. confluent cells cannot be used. Therefore, the elastic modulus of the overall cell can be attained with no distinction for the cell edge, cytoplasm, and nucleus.

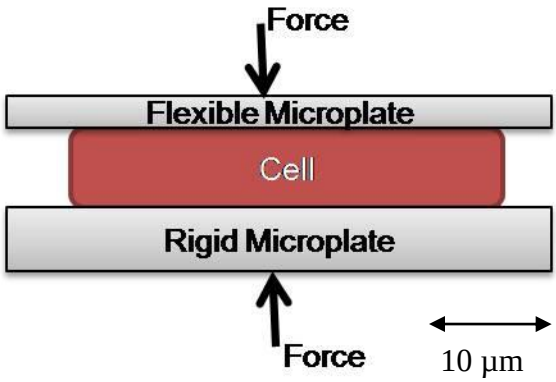

Figure 4. Microplates apply a nearly-uniaxial compression load to a single cell.

AFM Indentation

The AFM is a powerful microscopy technique that can provide morphology of living cells. AFM can also be utilized as an indenter to attain mechanical characteristics of cells (Radmacher, 1997). The AFM indentation is achieved with the use of a cantilever beam tip to indent a cell to measure the mechanical response of living cells. The theory behind the AFM indentation is that the cantilever works as a force sensor, i.e. with a known stiffness of the cantilever, its deflection and vertical displacement are related to underlying cell mechanical response (see Figure 5).

Various cantilever beams are utilized in the measurement of mechanical properties. One critical parameter, the spring constant of a given cantilever beam, is a function of the geometry and the elastic modulus of the cantilever. For example, a cantilever can consist of a 100-200 µm by 30-50 µm by 600 nm silicon nitride triangle attached to a larger SiNi chip that resembles a plank. At the tip of the cantilever, there is a sharp, pyramidal shaped tip 2.5-8 µm with a radius of 10-40 nm.

As seen in Figure 5, the cantilever beam is lowered in the direction of the z-axis to contact the cell and perform the indentation. The height data (z) and deflection (d) data are recorded during approach and retraction. The changes in deflection of the cantilever are recorded as slight movements of the laser reflection on the photodiode, which results in a measurement of deflection. The shake piezo measures finer changes in the z-axis resulting in topographical information of the sample. A force is calculated by the product of deflection with spring stiffness to attain force-indentation curves (F-δ). During an AFM indentation experiment, users can select the velocity at which the cantilever approaches the cell. This is important because the tip velocity controls the strain rate (change in deformation with respect to time), which is a determinant of the measured mechanical response of soft biological materials (Holzapfel and Ogden, 2006). In general, users are also provided with a "trigger" that allows the cantilever beam deflection to stop the approach and begin retreat. The retraction curve can be used in the analyses of time-dependent mechanical response, such as the difference between the approach-retract (hysteresis), which is an indication of time-dependent mechanical response. It is common to utilize the approach curve for the mechanical characterization of elastic properties of living cells (Azeloglu et al., 2008; Lin, Dimitriadis, & Horkay, 2007a, 2007b).

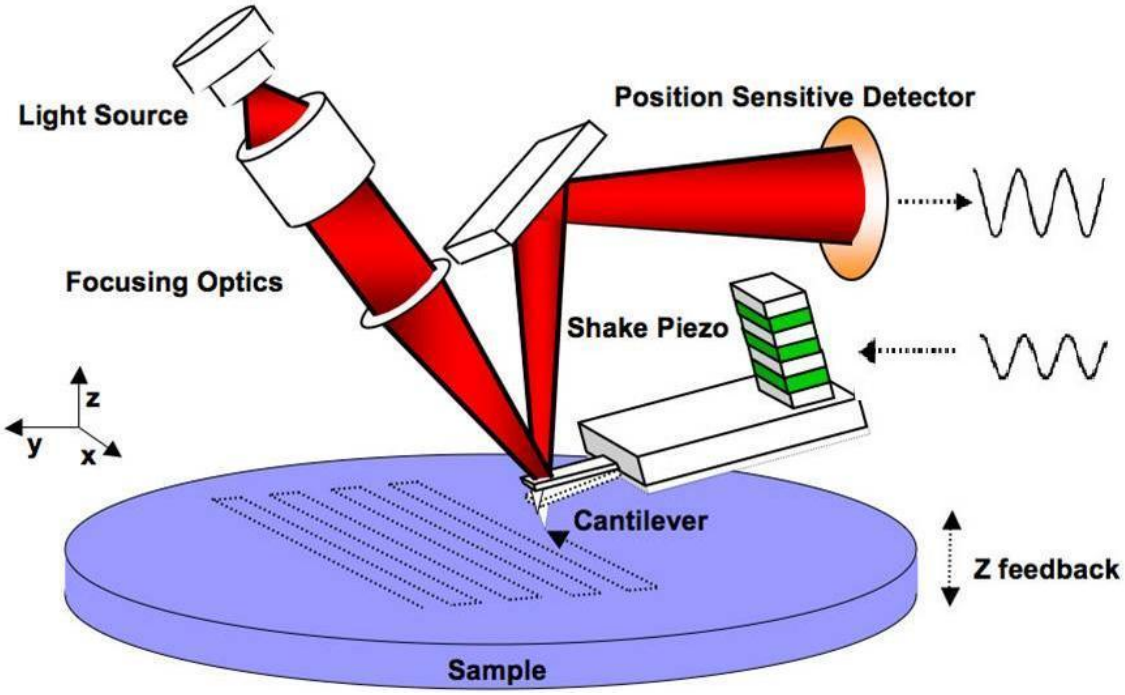

Figure 5. AFM Schematic. A light source (laser) is focused on the top surface of a flexible cantilever. The reflected light beam is captured by a position sensitive detector (image from Asylum Research, Santa Barbara, CA, used with permission).

Hertzian-Sneddon Approach for Analyzing Indentation

To calculate elastic modulus from F-δ curves, an appropriate indentation mechanics theory must be considered. The indentation mechanics of a spherical ball shape is studied by Heinrich Hertz in 1882. Hertz developed a model of the mechanical response of a homogenous, linearly elastic substrate with a spherical shape in contact. The Hertz theory was later adapted to conical indenters by Sneddon in 1965. The Hertz-Sneddon model is commonly used to evaluate cell elastic modulus from AFM F-δ measurements (Domke & Radmacher, 1998; Alcaraz et al., 2003; Rico, Alcaraz, Fredberg, & Navajas, 2005; Rico, Roca-Cusachs, Gavara, Farré, Rotger, & Navajas,

2005). In this indentation context, a relationship between the indentation depth (z-z_0-d) and the indentation force (k*d) is established, where z_o corresponds to the initial contact during the approach. The force resulting from a pyramidal indentation is calculated using

$$F = \frac{3E\ tan\ \alpha}{4(1-\nu^2)}\delta^2 \quad (1)$$

where F is the force defined as the product of spring constant (k) and the deflection (d), E is the elastic modulus, ν is Poisson's ratio, α is the half angle of the tip, and δ is the indentation experienced by the cell (Alcaraz et al., 2003; Radmacher, 2007; Sneddon, 1965). Cells are generally considered nearly incompressible (Radmacher, 1997). For incompressible materials, Poisson's ratio is assumed to equal 0.5. The cantilever beam deflection as a function of parameters obtained from AFM indentation measurements is expressed in equation 2.

$$d = \frac{3\ E\ tan\ \alpha}{4(1-\nu^2)k}(z - z_0 - d)^2 \quad (2)$$

For soft substrates, the Hertz-Sneddon model predicts a non-linear force curve near the contact region (Figure 6) (Radmacher , 2007). There are two reasons why non-linear force curves are present during the indentation of soft substrates: the geometry of the tip-contact region and the mechanical properties of the soft substrate. The geometry refers to the nonlinear relationship between the indentation depth and cross-sectional area of the contact region. When small indentations are considered, a reasonably realistic elastic modulus can be extracted or calculated. Moreover, the Hertz model assumes that the thickness of the substrate is infinite. However, the thicknesses of living cells as

substrates are far from infinite. The cells reside on materials of much greater elastic modulus when cultured. Therefore, as the indentation depth approaches the thickness of the cell in a given region, the cantilever begins to sense the elastic properties of the underlying culture dish. As a result, the measured elastic modulus is less reflective of the soft material's elastic response (Radmacher, 2007).

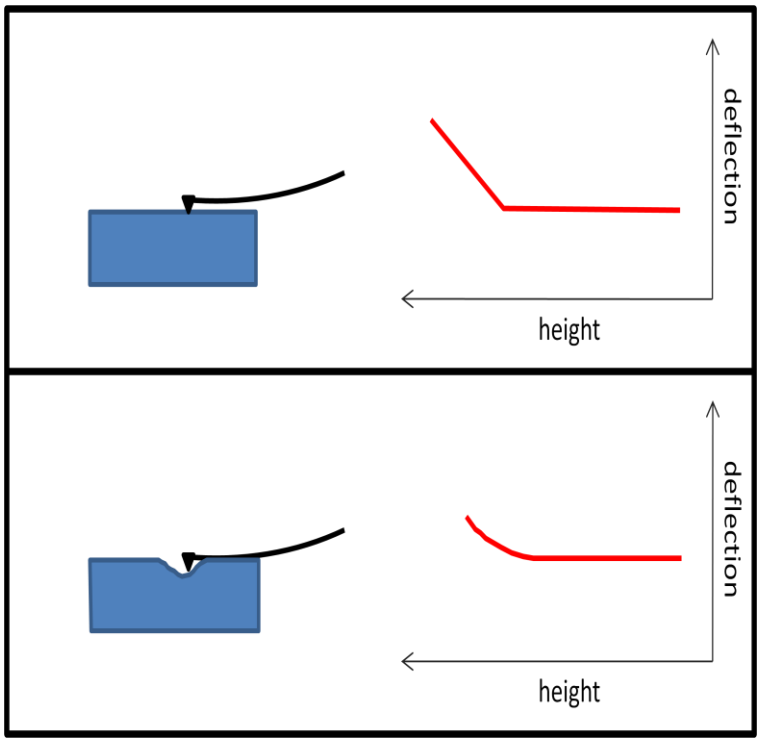

Figure 6. F-δ curves on a hard (top) and soft (bottom) substrate. TOP: The deflection is constant until the tip reaches the substrate and the point of contact is cleary visible. BOTTOM: The deflection is constant until the tip contacts the soft substrate and a gradual non-linear increase in deflection is evident.

The indentation depth for the determination of the elastic modulus is determined to be an important parameter. In Leonenko, Finot, & Amrein (2007), the elastic modulus is shown to be dependent on the indentation depth, as shown in Figure 7. Most of the elastic modulus curve is inversely dependent on the indentation depth (from ~200 nm and above), but there is a steep initial rise during an intitial indentation region. The study suggests that the initial elasticity between 100 nm and 200 nm of indentation is due to the measurements of the elastic modulus of the cytoplasm. According to this study, the

following measurements corresponding to greater than 200 nm indentation depths reflected the response of the whole cell. The figure shows that between an indentation depth of 300 nm and 500 nm there is a 10% decrease in elastic modulus.

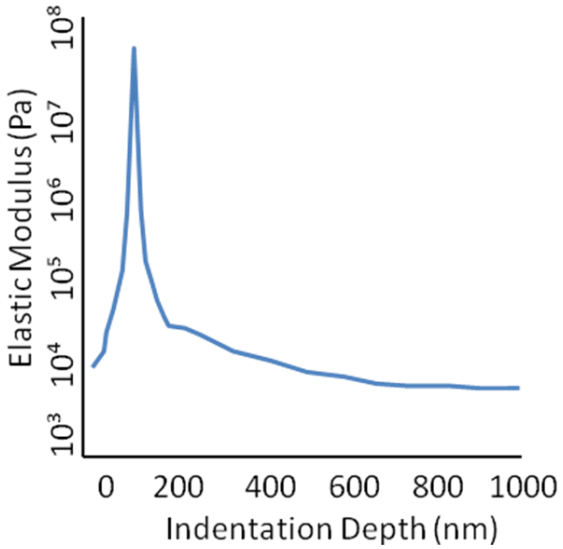

Figure 7. The elastic modulus of primary ATII cells versus the indentation depth of the AFM probe. The graph shows an initial higher elastic modulus portion for small indentations (adapted from Leonenko, Finot, and Amrein, 2007).

Non- Hertzian Approach for Analyzing Indentation

In order to overcome issues related to violations of Hertz-Sneddon contact assumptions, non-Hertzian approaches have been developed to analyze F-δ from AFM. One approach involves equations that describe the contact between the indenter and an isotropic (uniform in all directions), while accounting for the contribution of indenter geometry on the indentation depth (Costa, Sim, & Yin, 2006). Corrected for tip geometry, for a linearly elastic material, the elastic modulus is found to be independent of indentation depth. However, for non-linear and inhomogeneous materials, the elastic

modulus is dependent on the indentation depth (Costa et al., 2006). The contact region is modeled by a greater than second-degree polynomial (Adams and Nosonovsky, 2000). The challenges associated with the non-Herztian approach are the anisotropic (directional dependent) mechanical properties and dynamic architecture (Costa, Hucker, & Yin, 2002; Heidemann, Kaech, Buxbaum, & Matus, 1999; Maniotis, Chen, & Ingber, 1997) of the cell cytoskeleton.

Many AFM indentations at a given location can be performed in a raster mode in the X-Y direction to develop elastic modulus maps of the cell and surrounding cells. The size of the rastered region will determine the number of cells sampled. Users can select a scan rate, which is the rate that the cantilever moving in the X-Y direction. Sampling area and rate can also be controlled by the user, which are both controlled by the desire to reduce overall time for experimentation. Decreasing the total number of measurements decreases the time to complete a map; but, this has a negative impact on the resolution (Azeloglu etal., 2008)

In addition to force-indentation measurements, high-resolution topographical images can be produced in tapping mode where the cantilever nearly contacts the surface of the cell to determine topography. Topographical images can also be produced using the AFM in contact mode where the cantilever drags across the surface of a cell to determine morphology. The images produced are maps of the X-Y directions and a color bar is used to represent relative height change.

Advantages of AFM

The AFM is a powerful tool capable of producing high-resolution topographical images and measuring F-δ in aqueous solutions. This aqueous solution is generally used to maintain an environment similar to physiological conditions. From the perspective of mechanics, the AFM indentation is capable of measuring the mechanical response of the whole cell including the cytoplasm, cytoskeleton, nucleus, and cells' edges. Moreover, the AFM indentation resolution is fine enough to allow localization of mechanical responses to various cell regions, i.e. the nucleus. The cells need minor preparation for imaging or F-δ.

Disadvantages of AFM

A major challenge associated with the AFM indentation measurements is that interpretation of the cell indentation curves is a complex mechanics problem. It requires robust mechanical analysis to extract the underlying elastic modulus (Lin, Dimitriadis and Horkay, 2007a). Moreover, each AFM indentation curve exhibits sensitivity to vibrations and temperature fluctuations in the fluid surrounding the cells. Interactions between cells and the indenter can also introduce challenges to this technique (Lin et al., 2007b)

Alveolar Epithelial Mechanical Properties

In light of the capabilities and challenges associated with AFM indentation and other methods, many studies measuring the mechanical response of living cells have been published. Here, the focus is on cells related to the alveolar epithelium. For example, with the use of AFM indentation, it has been shown that primary Sprague Dawley neonatal rat ATII and primary ATI cells have an unequal elastic modulus of the cytoplasmic region, 4.7 ± 2.9 kPa vs. 2.5 ± 1.2 kPa, but the nuclear regions are not distinct statistically, 2.5±1.0 kPa in ATI vs. 3.1±1.5 kPa ATII (Azeloglu et al., 2008). In their studies, primary cells were isolated, cultured, labeled and measured. The difference in elastic modulus between the cytoplasmic region and the nuclear region of the ATII cells is suggested to originate from the presence of lamellar bodies found only in the cytoplasm of ATII cell (Azeloglu, Bhattacharya, and Costa, 2008). No characterization of mechanical properties by days in culture after isolation of primary cells was provided in these previous studies.

Table 1 is a summary of all the data found in literature with regards to any alveolar epithelial cell mechanical response. Testing techniques, data analysis method, indentation velocity and depth, cell type, cell region, and the elastic modulus of the measurements are included parameters in this table. MTC and OT mechanical characteristics are described with a shear modulus, *G*. To compare the shear modulus values to the elastic modulus values, the shear modulus is converted to an elastic modulus using the relationship between elastic constants. In general mechanics, the elastic modulus is the slope of the stress-strain curve in the elastic deformation region, the

pressure units are expressed as Pascals. Stress is equal to force over area and strain is change in the length over the original length. In indentation mechanics, the area of the force applied is changing as the object is indenting as in AFM F-δ measurements, making elastic modulus difficult to calculate. F-δ and the mathematical calculations to produce the elastic modulus is explored in the next sections. Figure 8 illustrates deflection of the cantielver and indentation of an ATII cell during a F-δ measurement.

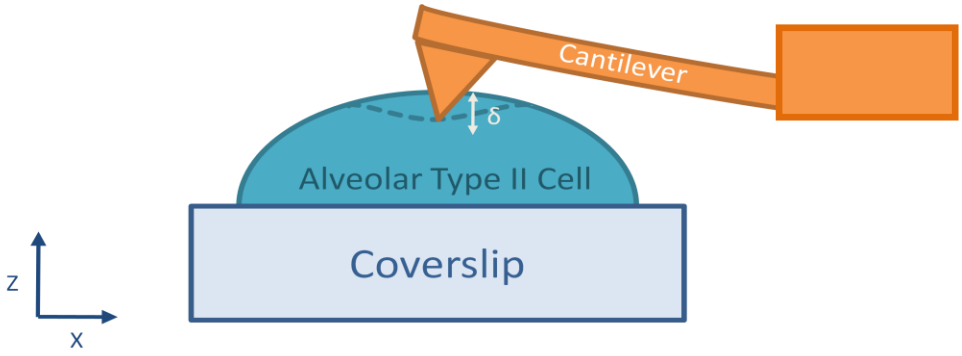

Figure 8. AFM Indentation. The cantilever with a known stiffness indents (δ is indentation depth) the cell. Using the indentation, cantilever stiffness, and Poisson's ratio, the elastic modulus can be extracted.

A number of studies presented in Table 1 have measured the elastic modulus of A549 cells, which belong to an adenocarcinoma cell line. These cells are considered to be similar to ATII cells because they include cytoplasmic lamellar bodies and produce surfactant proteins (Wang, Havil, Burns, & Sigmond 2007), but lack tight-junction formation capabilites as a monolayer (Kobayashi, Kondo, & Juni, 1995). Moreover, A549 cells are not able to transition to the ATI phenotype (Fuchs et al., 2003) and the morphology that is characteristic of the ATI cell can contribute to a change in mechanical characterization (Fuchs et al., 2003). The results of three mechanical characterization

studies of A549 cells are 1.59 ± 1.14 kPa, 1.38 ± 1.36 kPa, and 0.91 ± 0.47 kPa (Alcaraz et al., 2003; Rico, Alcaraz, Fredberg, & Navajas, 2005; Rico, Roca-Cusachs, Gavara, Farré, Rotger, & Navajas, 2005). The elastic modulus of A549 cells presented in these studies showed a smaller elastic modulus when compared to the primary ATII cells.

The summary in Table 1 includes some important differences in testing technique. The indentation velocity of the cantilever tip varies from 10 μm/s to 1.8 μm/s. The velocity of the cantilever can have an effect on the measurement of elastic modulus. The indentation depth also varies from 300 nm to 1600 nm, the increased indentation depth can result in substrate effects on the measured elastic modulus. Also, using MTC, Berrios et al. (2001) is able the show that there is a slight increase in shear modulus or apparent elastic modulus of primary rat ATII cells over days 2 through 4;however, the increase is not statistically significant.

In this thesis, the AFM indentation is the chosen method to characterize the mechanical properties of cells of ATII cells because the AFM has the capability to measure localized mechanical responses of cells. Moreover, the AFM allows the mechanical characterization of cells in culture media.

Table 1. *Summary of Alveolar Epithelial Cell Mechanical Properties in Literature.* Rows correspond to the cell type whereas the columns correspond to the mechanical characterization method. The values are mean elastic modulus in Pa. The MTC data is converted to elastic modulus from the apparent G'. The region is the area of interest within the cell (Alcaraz et al., 2003; Berrios et al., 2001; Azeloglu et al., 2008; Laurent et al., 2002; Rico et al., 2005; Trepat et al., 2004). *Adapted from G shear modulus to E elastic modulus.

Author	Geometry	Measurement	Data Analysis	δ Velocity	δ Depth	Cell Type	Region	E (kPa)	±
Azeloglu et al (2008)	Pyramid	AFM	E, Non-Hertzian	10 μm/s	300 nm	ATII d2	cytoplasm	4.7	2.9
							nuclear	3.1	1.5
						ATI	cytoplasm	2.5	1.2
							nuclear	2.5	1.0
Alcaraz et al (2003)			E, Hertzian-Sneddon	6 μm/s	800-1600	A549	whole cell	1.6	1.1
Rico et al (2005a)				1.8 μm/s	~20% of			1.4	1.4
Rico et al (2005b)				NA	500 nm			0.91	0.47
	Sphere							0.47	0.18
Laurent et al (2002)*	Sphere	OC	G	NA			cytoplasm	0.38	0.22
		MTC						0.14	0.02
Trepat et al (2005)*								1.2	0.11
Berrios et al (2001)*						ATII d2		0.45	0.08
						ATII d3		0.52	0.20
						ATII d4		0.68	0.05

Literature Review and Background Conclusions

In light of a thorough literature review, the following conclusions are drawn.

i. There is a gap in literature of the mechanical characteristics of ATII cells as a function of culture time, which can be indicative of the timeline associated with the dedifferentiation of primary ATII cells into ATI-like cells.

ii. The AFM indentation is a valid method to characterize the mechanical properties of ATII cells because the AFM has the capability to measure the mechanical response of the cell in either in a localized or average manner.

iii. The Hertzian-Sneddon model is used in many AFM for indentation studies (Alcaraz et al., 2003; Berdyyeva, Woodworth, & Sokolov, 2005; Radmacher, 2007) and is well-suited for the scope of this thesis research effort.

These conclusions are used as the rationale for the study of mechanical properties of alveolar epithelial cells. The hypothesis of the work presented in this thesis is that the elastic modulus of ATII cells, obtained with the use AFM indentation technique, exhibit a dependence on culture time.

Chapter 3: Materials and Methods

In order to measure the mechanical properties of primary ATII cells, cells were isolated and cultured. Then, AFM indentation experiments were conducted, followed by data analyses.

Alveolar Epithelial Type II Cells

The ATII cells were isolated eight times at the University of Tennessee Health Sciences Center (UTHSC), Memphis, TN. The cells were then plated at either UTHSC or at the University of Memphis (UM) for further testing.

Isolation

ATII cell isolations took place at the UTHSC under the direction of Dr. Christopher M. Waters. The isolation and culture of primary Sprague-Dawley rat ATII cells were completed according to established techniques described by Dobbs, LG et al. (1986, 1990).

The isolated ATII cells were resuspended in *culture medium* without FBS [DMEM, 4 mM glutamine, 1% penicillin/streptomycin, and 0.25 µM amphotericin B (Sigma, St Louis, MO)] at a cell density of 3.5 X 10^6 cells/ml. After the cells were suspended, they were plated at the UTHSC for isolations 1-2 and were plated at UM for isolations 3-8. Table 2 demonstrates the differences between each of the eight isolations.

For isolations 3-8, the cells were transported in *culture medium* in capped plastic centrifuge tubes and carefully driven approximately 5 miles to the University of Memphis where the AFM is housed. These ATII cells were then plated immediately upon arrival at UM.

Plating

The ATII cells were counted using a hemacytometer on isolation 4 to confirm that the seeding density was 3.5 X 10^6 cells/ml. Cell counting for isolations 1-3 and 5-8 was performed by another researcher at UTHSC. Inside of a cell culture hood, 1 ml of cell stock was seeded on glass coverslips [30 mm x 1 mm; circular (Asylum Research, Santa Barbara, CA)], on which an RLF-6 basement matrix was deposited via culture of RLF-6 cells. The cover slips were next placed inside of 30 mm petri dishes and 1.5 ml of *culture medium* with 10% FBS was added to the petri dish. Following, the cells were placed inside of a 37°C 5% CO_2 incubator for 40 hours then the *culture medium* was changed and the plates were incubated for another 8-10 hours. Finally, the ATII cells were checked for confluence with the use of light microscopy, which was when 100% of the coverslip was covered by cells.

Table 2. *Cell Culture and F-δ Information for Each Isolation*.

<table>
<tr><th>Isolation</th><th>Isolation Location</th><th>Cell Count</th><th>Seeding Location</th><th>Transportation</th><th>Media Change</th><th>Confluent</th><th>Determine Cantilever Spring Constant (k)</th><th>Force Map Utility</th><th>DefVolts Trigger (V)</th><th>δ Velocity (µm/s)</th><th>Map Size (µm x µm)</th><th>F-δ Curves per Map</th></tr>
<tr><td>iso1</td><td rowspan="8">UTHSC</td><td rowspan="3">UTHSC</td><td rowspan="2">UTHSC</td><td rowspan="2">Styrofoam cooler, car, plated on glass coverslips</td><td rowspan="8">AM d2</td><td>PM d2</td><td rowspan="8">Thermal Tune</td><td rowspan="3">Chad</td><td rowspan="8">1.2</td><td rowspan="8">1.03</td><td rowspan="3">30 x 30</td><td rowspan="3">100</td></tr>
<tr><td>iso2</td><td>PM d3</td></tr>
<tr><td>iso3</td><td rowspan="5">UM</td><td rowspan="5">Styrofoam cooler, car, capped centrifuge tube</td><td rowspan="4">PM d2</td></tr>
<tr><td>iso4</td><td rowspan="5">UM</td><td rowspan="2">IGOR</td><td>32 x 32</td><td>1024</td></tr>
<tr><td>iso5</td><td rowspan="4">UTHSC</td></tr>
<tr><td>iso6</td><td>Chad</td><td>20 x 20</td><td>400</td></tr>
<tr><td>iso7</td><td rowspan="2">IGOR</td><td rowspan="2">32 x 32</td><td rowspan="2">1024</td></tr>
<tr><td>iso8</td><td>No</td></tr>
</table>

AM: Morning PM: Evening

Abbreviations

UM: University of Memphis UTHSC: University of Tennessee Health Sciences Center

Chad: Simple mapping utility IGOR: Upgraded mapping utility (Wavemetrics, Lake Oswego, OR)

Preparation of ATII Cells for AFM

The coverslip containing the ATII cells was removed from the incubator located two floors away from the AFM and the cells were checked for 100% confluence at 100X magnification on an inverted microscope (Nikon TMS, Japan). After confirming confluence, the coverslip of cells, along with a 5mL aliquot of complete media, was brought to the AFM. Once in the AFM room, the excess media from the coverslip was removed with bulb suction with a glass pipette and the coverslip was carefully removed from the petri dish. To accomplish this, a 1.5mm diameter drill bit was twisted by hand to bore a hole in the bottom of the petri dish to elevate the glass coverslip from the bottom of the petri dish. The coverslip was then gently removed from the petri dish with a pair of tweezers, while elevating the coverslip with the drill bit. The coverslip was then placed on the closed fluid cell kit coverslip holder and 18 drops of media (~1 ml) were slowly placed on top of the ATII cells forming a meniscus, due to the surface tension of the media, across the coverslip (Figure 9).

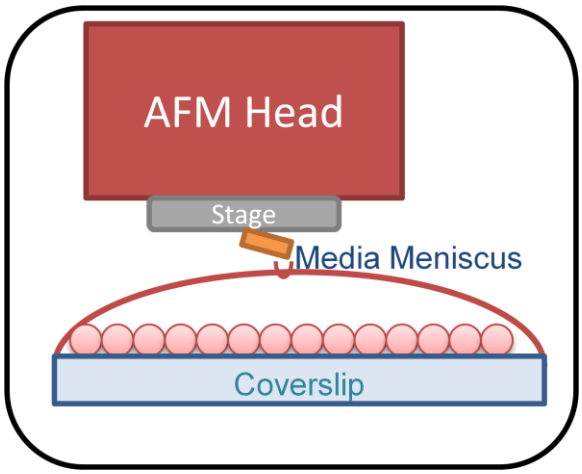

Figure 9. A schematic depicting side view of the AFM head with cantilever beam (gold) shows the drop of media and the cantilever meniscus. The coverslip was shown with cells (circles) and its media meniscus above. The two menisci must meet to have the cantilever appropriately cross the surface tension created by the media meniscus.

AFM Measurements

AFM Calibration and Start Sequence

An AFM MFP-3D standalone unit (Asylum Research, Santa Barbara, CA) with the IGOR software (Wavemetrics, Lake Oswego, OR) was used for all AFM imaging and AFM F-δ measurements. First, the AFM laser was turned on; the laser was allowed to stabilize over the course of 20 minutes. The illuminator light was turned on during this time to provide light to the camera attached to the AFM stage. In addition, power was turned on to the TS-150 Table stabilizer (Herzan, Laguna Hills, CA) which maintains a level stage and provides vibration isolation for the AFM (Figure 10). The IGOR software

environment supports the user with tools to control the AFM as well as scientific graphing, data analysis and image processing. A new template for experimental controls was selected for each experiment and subsequently, each experiment was saved under a different file name.

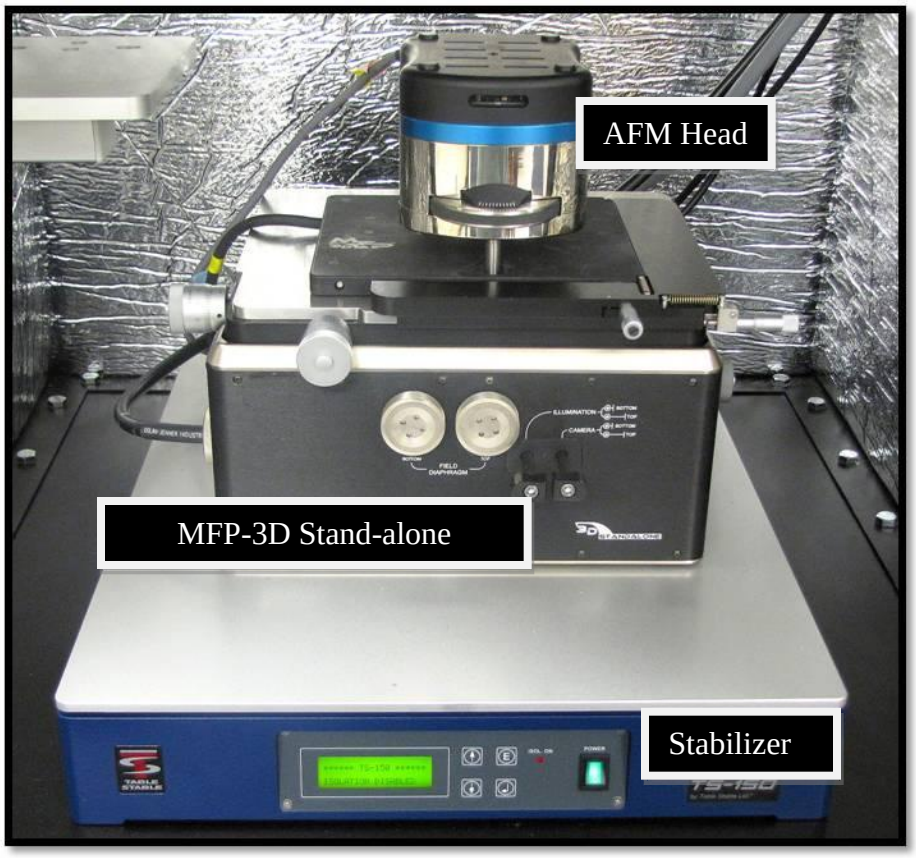

Figure 10. AFM Assembly. TOP: AFM Head. MIDDLE: MFP-3D Standalone unit. BOTTOM: Stabilizer. The AFM was contained within a vibration-reduction chamber.

A silicon nitride DNP-S cantilever (Veeco, Plainview, NY) was placed on the cantilever holder (Figure 11) by adjusting the screw holding the silver-colored holding plate to hold the cantilever chip in place. The cantilever chip and cantilever holder were then placed on the underside of the AFM head and secured into place using the spring-

loaded mechanism that accompanies the AFM head. The AFM head was then overturned onto the stage with the three legs of the AFM head being placed into their associated leg holders on the AFM stage.

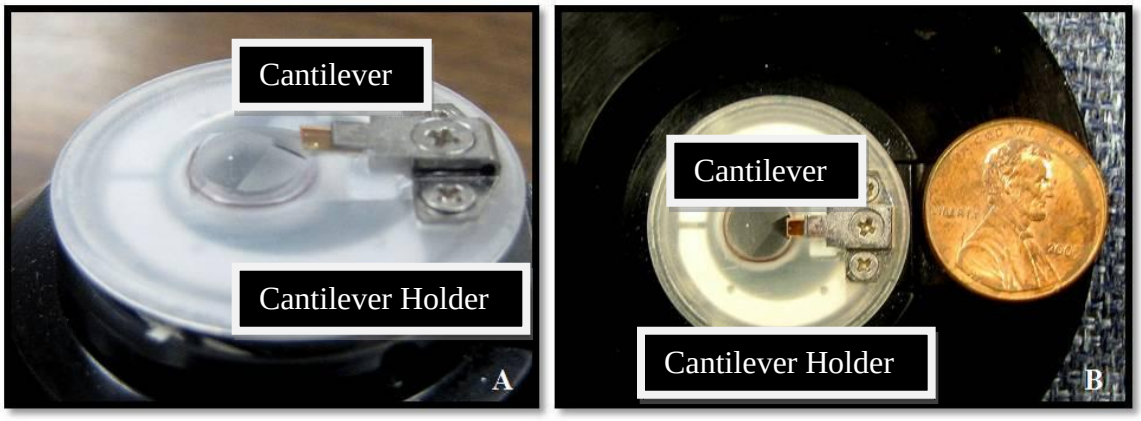

Figure 11. The cantilever holder (white) with the DNP-S cantilever (gold) secured under the holding plate by three screws.

Spring Constant Measurement

The AFM's integrated camera was used to view the cantilever on the cantilever holder. At times, one chip contained multiple cantilever beams. In such cases, the laser was focused on the wider, longer cantilever, which corresponded to a lower spring constant value as opposed to the smaller, shorter cantilever, which has a larger spring constant. The laser beam was reflected off the gold coating on the cantilever into a mirror, and then focused on the center of the photodiode, which maximizes the "sum." The sum was the total amount of light collected by the photodiode in volts, usually to about 6V. The sum was maximized by adjusting the X and Y stages on the AFM head. The deflection of the cantilever was adjusted to 0.0 ± 0.5V. An Asylum add-on package

for the IGOR software was then used to find the resonant frequency of the cantilever, which was needed to calculate the spring constant of the cantilever tip. The nominal spring constant was 0.06 N/m.

Cantilever in Fluid

The AFM head was lifted, and the coverslip holder was placed on the stage (Figure 12). The AFM head was then placed with the legs pointed upward and the cantilever visible. Then, a small drop of media was placed on the cantilever tip, taking care to neither touch the cantilever tip nor spill the liquid into the AFM head. The small drop was placed such that, it forms a meniscus on the cantilever. The AFM head was then carefully turned with the legs pointed downward and placed on the stage with the back two legs inserted first and the front leg slowly lowered until the meniscus from the cantilever and the meniscus from the coverslips meet. These steps prevent an air bubble from entering and altering the angle of the cantilever tip. Next, the AFM, cantilever, and cells were left to rest for 15 minutes while the temperature of the cantilever and the media equilibrates, or until the deflection of the cantilever remains constant.

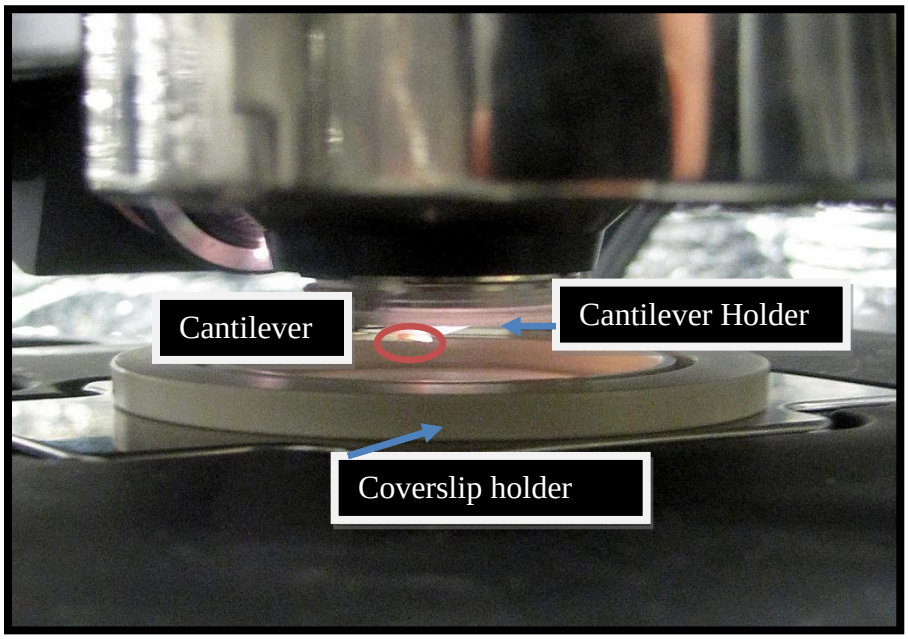

Figure 12. Close-up picture of the AFM head with the coverslip holder. Coverslip holder (beige) was located in the standalone unit and the cantilever (circle) in the cantilever holder on the AFM head was lowered to meet the coverslip. The ATII cells were placed on a coverslip within the coverslip holder.

After submerging the cantilever in the *culture medium*, the AFM laser was no longer focused on the cantilever and was adjusted to account for the change in the light refraction associated with moving from air to water. Again, the summing signal of the photodiode was maximized. The front wheel was used to lower the AFM head until the LVDT Z-axis voltage was near 70 V. During the lowering, the ATII cells on the coverslip came into focus. The thermal calibration process was performed again and the spring constant of the cantilever was measured in fluid as well.

AFM F-δ

The parameters for the F-δ curves are found in Table 2. The trigger was set to DefVolts (deflection voltage). The velocity of the cantilever in the X or Y direction, known as scan rate, was 30 µm/s. The velocity of the cantilever in the Z- direction was set to 1.03 µm/s. The *z* and *d* values are recorded approximately every 0.5 to 1 nm. The maps of cells had resolutions of 100 pixels, 400 pixels, or 1024 pixels (Wagh et al., 2008), each pixel represented a single elastic modulus value. The maps were over areas of 100 µm², 400 µm² or 1024 µm². The time to complete one 1024 curve scan was 35 minutes. A maximum of two scans were run for each coverslip of ATII cells. The resulting F-δ curves were exported as IGOR binary files (Wavemetrics, Lake Oswego, OR) in order to be analyzed by the MATLAB (Mathworks, Natick, MA; v 2009a) program for validity, contact point, and elastic modulus using the calibrated spring constant value.

AFM Imaging

The ATII cells were imaged in contact mode, using a 1200 mV amplitude set point, (which controls the maximum amplitude of cantilever via the voltage that the piezo can move), a drive amplitude (the amplitude of the voltage applied to the piezo that drives the cantilever) of 800 mV, and an integral gain near 10, which controls the response time of the feedback loop. The image was 60 x 60 µm with a scan rate of 0.5 Hz. The time to complete one scan was 8.5 minutes. The set point, integral gain, drive amplitude, and scan rate were adjusted to reduce noise. The trace and retrace lines during

imaging describe the forward and backward movement of the cantilever over the same line over the cell (Figure 5).

Elastic Modulus Computation

The force measurements were analyzed using a MATLAB (Mathworks, Natick, MA) program written by Esra Roan, PhD.

The major steps of the MATLAB program were:

1. Imports deflection and LVDT (height) information;
2. Removes auxiliary zeros;
3. Separates the approach and retraction curves;
4. Smoothes curves;
5. Removes curves with fewer than three data points in the indentation region;
6. Searches for a contact point;
7. Uses the Hertz-Sneddon model (equation 2) to extract the elastic modulus using; fminsearch (non-derivative optimization);
8. Averages the elastic modulus;
9. Constructs an elastic modulus map (see next section).

Fminsearch is a function provided by MATLAB that utilizes (Fminsearch MATLAB Function Reference, 2010) Nelder-Mead non-derivative optimization (best solution) (Nelder & Mead, 1965). This function uses a direct local search to minimize the residuals (distance deviation between the best-fit curve and the F-δ data) and determine a

line of best fit. An initial guess of elastic modulus is required, in this case 1 kPa to create an initial simplex of N+1 points, where N was the dimension of the problem. In the Hertz contact model, the dimension was one, the elastic modulus (Lagarias, Reeds, Wright, & Wright, 1998) that is estimated by fitting equation 2. The simplex was constantly refined to locate the minima and then to reduce the size of the simplex until the residuals were minimized (Lagarias et al., 1998). The resulting model from fminsearch was then checked for visual fit to the F-δ data to assure a reasonable representation of the measurement by fitting the curve.

User controlled functions of the MATLAB program were:

1. Controlling the R^2, i.e. goodness of fit, values greater than 0.90;
2. Setting a maximum possible elastic modulus;
3. Selecting an indentation depth.

The maximum value of accepted elastic modulus for the calculation of final mean of elastic modulus values, a user input into the MATLAB program, was varied (30kPa and 100kPa) along with the indentation depth (200nm, 300nm, and 500 nm). The elastic modulus and indentation depth was varied to reduce the potential inclusion of substrate effects to the measurements. In the final reported values, a maximum value of 30 kPa was chosen because typical elastic modulus values for living cells are found to be less than 30 kPa. The curves were analyzed for visual quality of fit, along with maximum allowable elastic modulus and indentation depth.

The program includes reducing the elastic modulus by 10% to account for the overestimation based on the finding by Leonenko et al. (Figure 7) for indentation depths

of 300 nm. The indentation depth of 500 nm was considered appropriate for measuring the mechanical properties of the whole cell, but 500 nm was a large indentation depth if the cell has a region with a height of one micron. Therefore, the indentation depth does not follow the Hertz assumption of a small indentation. An indentation depth of 300 nm was selected for this thesis.

Mapping

To display the many measured values of the elastic modulus, maps were generated using the MATLAB program. The MATLAB program calls the elastic modulus for each curve in a force map to be mapped on a 2-D surface corresponding to the location that the curve was taken relative to the other curves in a single force map. A record of the F-δ curves was essential to the completion of the elastic modulus map. The record was necessary in order to form the elastic modulus maps by taking a string of elastic modulus values and converting the values into a map. The map was constructed by concatenating the array of values in to a matrix. If a record was not kept of the order of the string or the start point, the maps were not useful because the map would not be able to relate the 2-D areas properly if the start point was not accurate. The elastic moduli for each map were averaged and standard deviations for each map were recorded.

Statistical Analysis

A non-parametric test was performed to evaluate if there was a significant difference between days 2 and 3 in culture. The non-parametric test selected was a Mann-Whitney U test. The test determined if the two independent samples (days 2 and 3) were from the same sample distribution (null hypothesis) or from statistically different distributions (alternative hypothesis). The test was selected because the samples had two different values of n, the number of individual elastic modulus measurements. The α value of the test was 0.05 for a two-sided test.

Chapter 4: Results

The results include the plating of alveolar epithelial type II cells, the calibration, F-δ, and imaging using the AFM to test ATII cells, the data analysis using MATLAB to find the elastic modulus and create elastic modulus maps, and the data analysis using mean, standard deviation, and Mann-Whitney non-parametric test to quantify the information.

Alveolar Epithelial Type II Cells

Plating

The ATII cells were counted using a hemacytometer on isolation 4 and the cell density was 3.35 X 10^6 cells/ml, to confirm that the seeding density was 93% of the expected value, 3.6 X 10^6 cells/ml. Isolations 1-3 and 5-8 the cells were counted, and then media was added to the cells for a final density of 3.6 X 10^6 cells/ml, the cells were not recounted again. Forty-eight hours after seeding the cells, the confluence was determined to be 100% or the cells were given several more hours to become confluent. If confluence was not reached, F-δ measurements were not performed. See Table 2 for specific isolation information.

AFM Measurements

AFM Calibration

During the AFM set-up, the cantilever was calibrated to determine the spring constant and resonant frequency. The calibration was conducted with an automated utility of the IGOR software. The spring constant was the *k* value used to calculate force using the cantilever deflection and the mean *k* value was 0.03 ± 0.01 N/m. The *k* values for each isolation and day were found in Table 3. The NC value in isolation 2 was due to the cells not becoming confluent until the third day. The TFC values in isolations 3-8 were due to too few coverslips of confluent cells.

Table 3. *Isolation and Day Summary*. The table represents the isolations by columns and the number of days post isolation by rows that were completed. The spring constant values for all cantilevers fell within the cantilever manufacturer range. *This was *k* value was distinctive because a cantilever with a higher nominal spring constant was used.

k=N/m	**iso1**	**iso2**	**iso3**	**iso4**	**iso5**	**iso6**	**iso7**	**iso8**
Day 2	0.01285	NC	0.02489	0.02217	0.01144	0.03071	0.03042	0.02542
Day 3	0.02968	0.01676	TFC	TFC	TFC	0.03883	0.0291	0.06844
Day 4	0.10804*	0.02432	TFC	TFC	TFC	TFC	TFC	TFC

Abbreviations iso: isolation

NC: Not Confluent TFC: Too Few Coverslips

AFM F-δ

Indentation experiments were performed on square areas with confluent ATII cells. The curves were exported from IGOR to comma separated values files as both the approach and retraction curves. Examples of these two types of curves are available in Figure 13. The MATLAB program searches for the contact region of the approach curve to extract the elastic modulus. The contact point was found by calling the point when the height and deflection change from zero to a positive number.

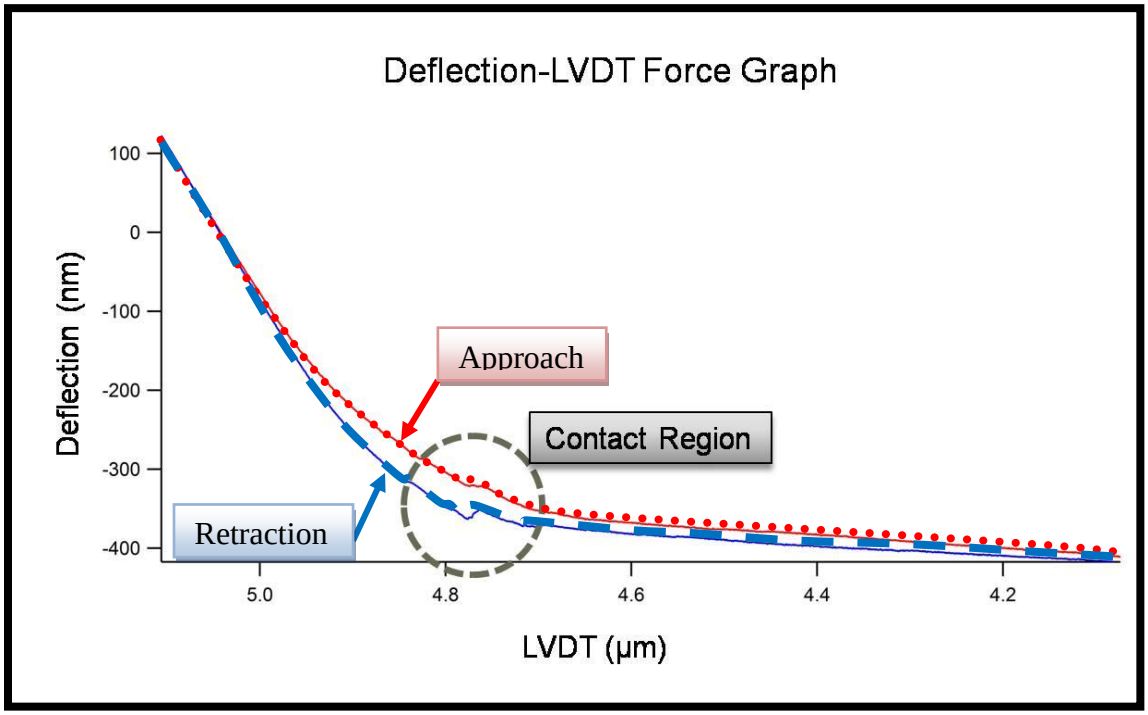

Figure 13. IGOR raw data. Deflection was recorded on the vertical axis and LVDT or z-axis change was recorded on the horizontal axis. The horizontal axis shows a decrease in LVDT. The circled region highlights the area where the cantilever was begins to and ceases to contact the cell. The small amount of deflection prior to the cantilever contacting the cell was from the fluid interaction with the cantilever.

AFM Imaging

A topographical height image of an ATII cell field (Figure 14) shows the live ATII cell in *culture media*. Three different sizes of images were shown 90 x 90 µm (top), 60 x 60 µm (middle), and 30 x 30 µm (bottom). The maps show different levels of detail the largest map shows the arrangement of cells, the middle map suggests that the nuclear regions are the higher portions of the maps, and the map covering the smallest area shows the nuclear region and cell morphology. The images were taken from different sections of a coverslip with confluent ATII cells. The color bar reflects the relative height of the cells in the image.

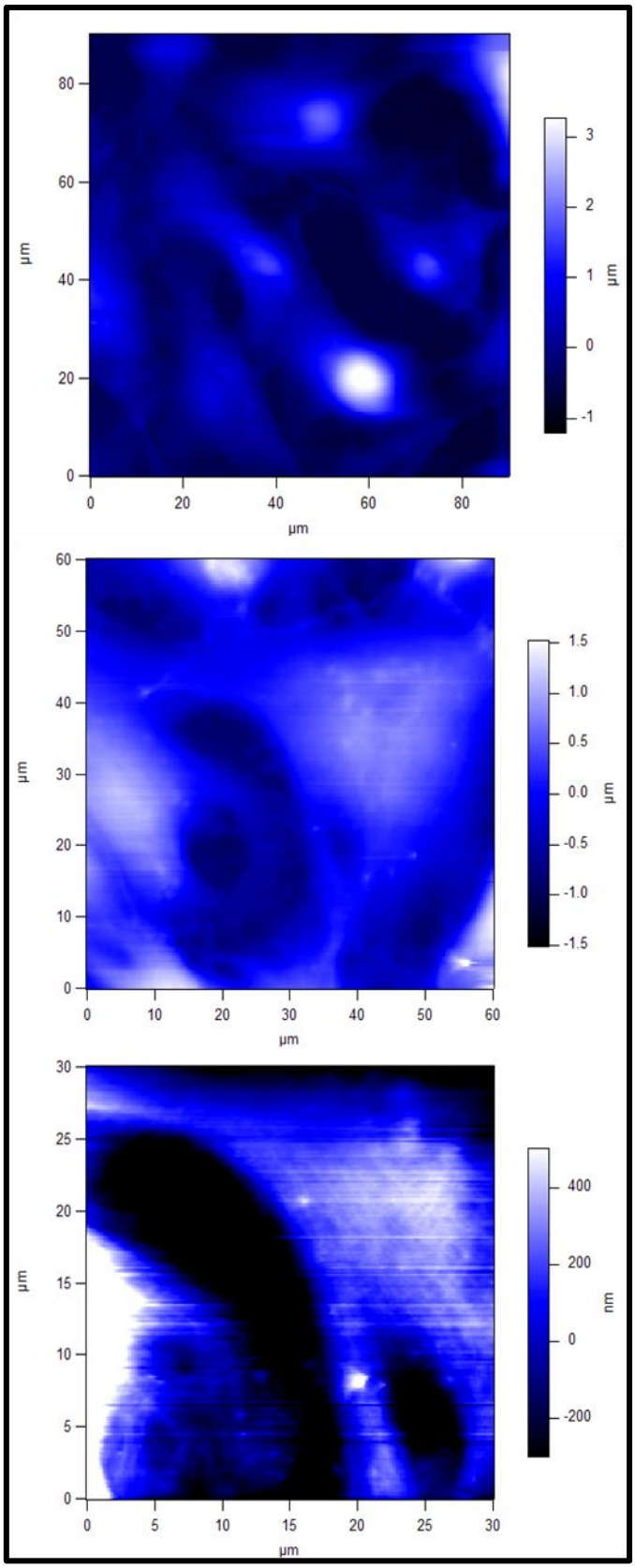

Figure 14. Topographical images obtained using an AFM with a DNP-S cantilever (Veeco, Plainview, NY) in contact mode with a scan rate of 0.5 Hz, a spring constant of 0.05 N/m and Day 2 of live primary ATII cells. The color bar reflects the relative height changes of the image. The x and y axis were in microns and represent a 90 x 90 µm (top), 60 x 60 µm (middle), and 30 x 30 µm (bottom) map of the confluent ATII cells.

Elastic Modulus Computation

The MATLAB program was run with user input variables including variations of the maximum accepted elastic modulus and the acceptable indentation. In the study Leonenko et al., the authors showed that an indentation depth of 200 nm was measuring the elastic modulus of the plasma membrane and not the whole cell. The indentation depth of 500 nm was too large in the thinner portions of the cell. Therefore, an indentation depth of 300nm was used for all subsequent elastic modulus extractions (Appendix A). The best fit curves from the MATLAB program were also visually checked to determine that the global minimum was found as opposed to a local minimum (Figure 15). The maximum accepted elastic modulus user input showed that when the maximum was set to 100kPa, the standard deviation of the mean was greater than the mean. In the study, Leonenko et al, the optimum indentation depth was 500 nm and when the elastic modulus for both the 300 nm and 500 nm marks were compared, there was a 10% decrease in elastic modulus. Therefore, the elastic modulus values in the MATLAB program were decreased by 10% (Leonenko et al., 2007) to correct the values to an indentation of 500nm, which accurately estimates the elastic modulus of the whole cell.

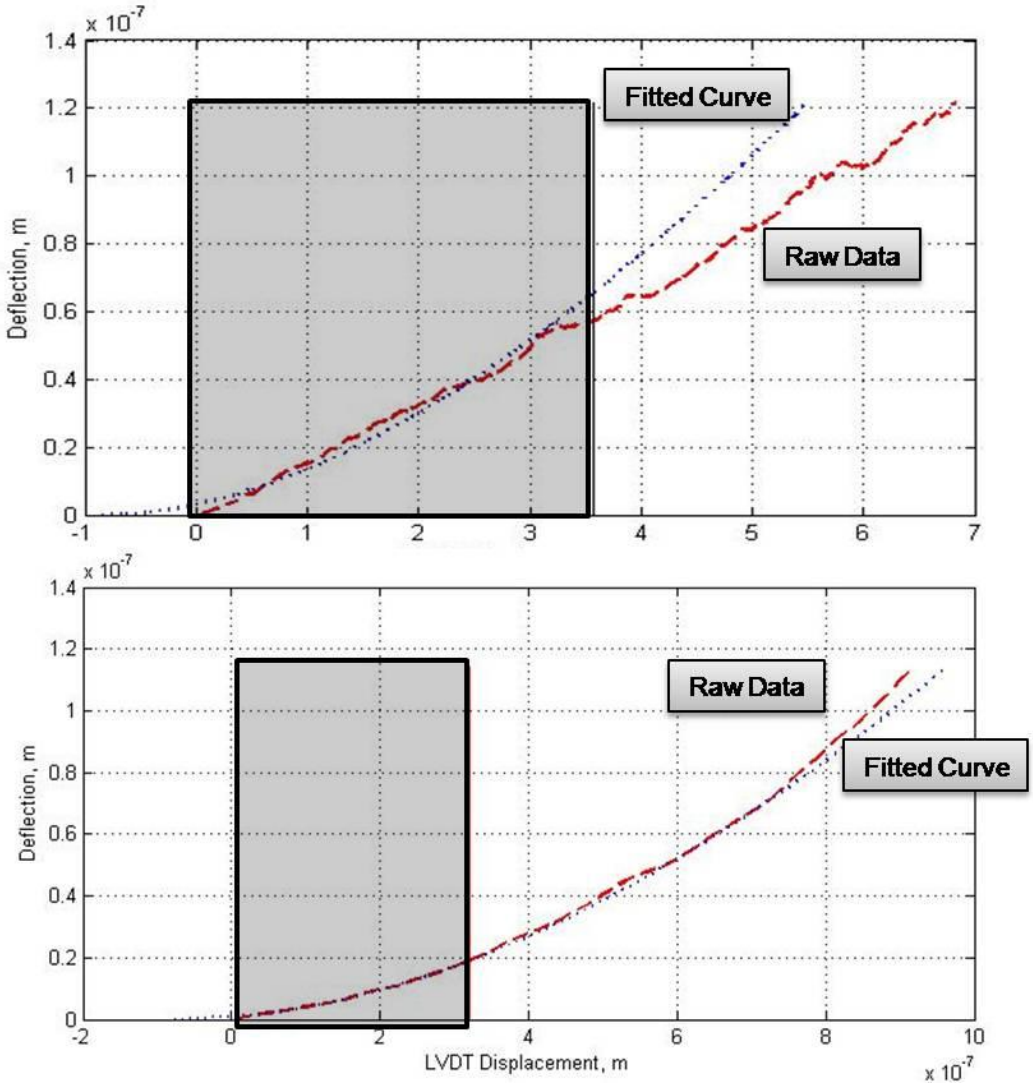

Figure 15. Examples of Fitted Curves. The shaded region was the indentation region over which the curve was analyzed. The x axis was LVDT displacement corrected to zero and the y-axis was deflection. The x axis shows an increase in LVDT displacement. The top graph shows a poor fit with a pre-contacted cantilever (elastic modulus was 16 kPa). The bottom graph shows a contact point (elastic modulus 5.8 kPa). The R^2 value for both graphs was greater than 0.99. The visual inspection of the gray boxed regions shows that the line of best fit and the raw data more clearly correlates in the bottom graph when compared to the top graph.

Mapping

The elastic modulus maps were obtained by assigning the X-Y vertical scanning coordinates and the corresponding F-δ curves to pixels and assigning the calculated the elastic modulus values to colors (Figures 16, 17, and 19). Not all values of elastic moduli were accepted. In this document, "reviewed" refers to a matrix of F-δ curves that have undergone elimination, i.e., accepted or eliminated F-δ curves. The white pixels in the elastic modulus maps show the measured values of moduli that were eliminated. The possible reasons for not accepting a curve were: exceeds the maximum accepted elastic modulus, poor fit or R^2 value, or less than three points of data within the indentation depth. The histograms show the relative distribution of elastic moduli over the maps.

A

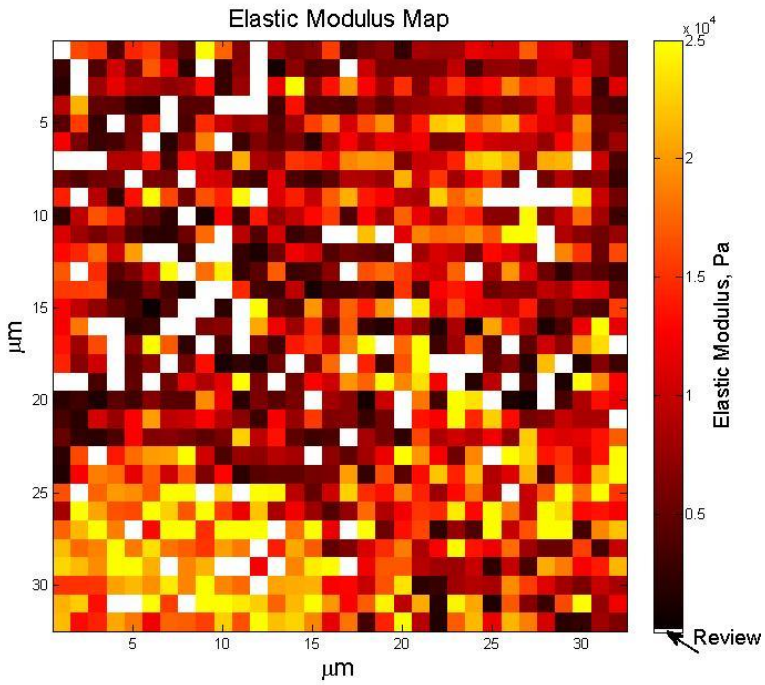

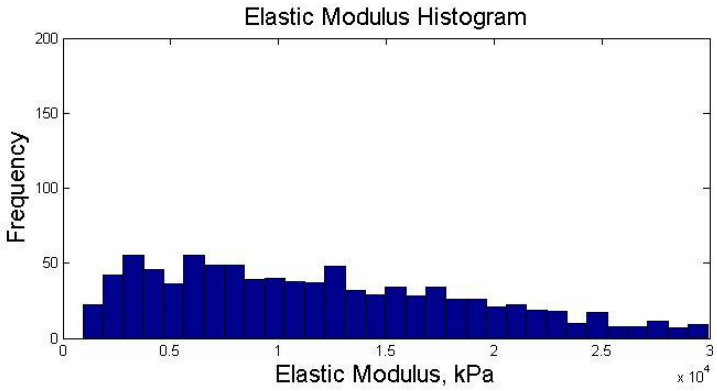

B

Figure 16. Iso5d2 Elastic Modulus Map and Histogram A: The map was an X-Y directions map that corresponds with the histogram represented below, the map represents raster scan of the confluent ATII cell field. The white pixels (squares) represent the curves that were reviewed based on fit to Hertz model, maximum elastic modulus, or standard deviation. The color bar represents the elastic modulus with darker pixels having a smaller elastic modulus when compared to the lighter colored pixels. B: The elastic modulus histogram corresponds with the elastic modulus graph. The frequency of the occurrence of the elastic modulus was the y-axis and the elastic modulus ranges were the x-axis.

Figure 16 illustrates pixels or curves that were reviewed that appear to have no pattern across the elastic modulus map. There appears to be areas of high elastic modulus surrounding the reviewed curves as well as low elastic modulus. Figure 17 contrasts Figure 16 because the reviewed curves tend to be located to a region and not dispersed throughout the entire map. Figure 17 shows a much smaller area (400 vs. 1024 μm^2) but the pixel size represented the same area, 1 μm^2. Figures 16, 17, and 18 elastic modulus maps show areas of high and low elastic modulus that tend to group together in regions. Figure 18 shows few reviewed curves; therefore, the acceptance percentage (accepted/attempted curves) was much higher (Figure 19). The elastic modulus maps in Figure 18 show a gradual increase and decrease of elastic modulus over the maps with a clear regional correlation of high and low elastic modulus. The histograms found in figure 18 show a variety of distributions. The average elastic modulus for each map found in figures 16-18 is found in Table 4.

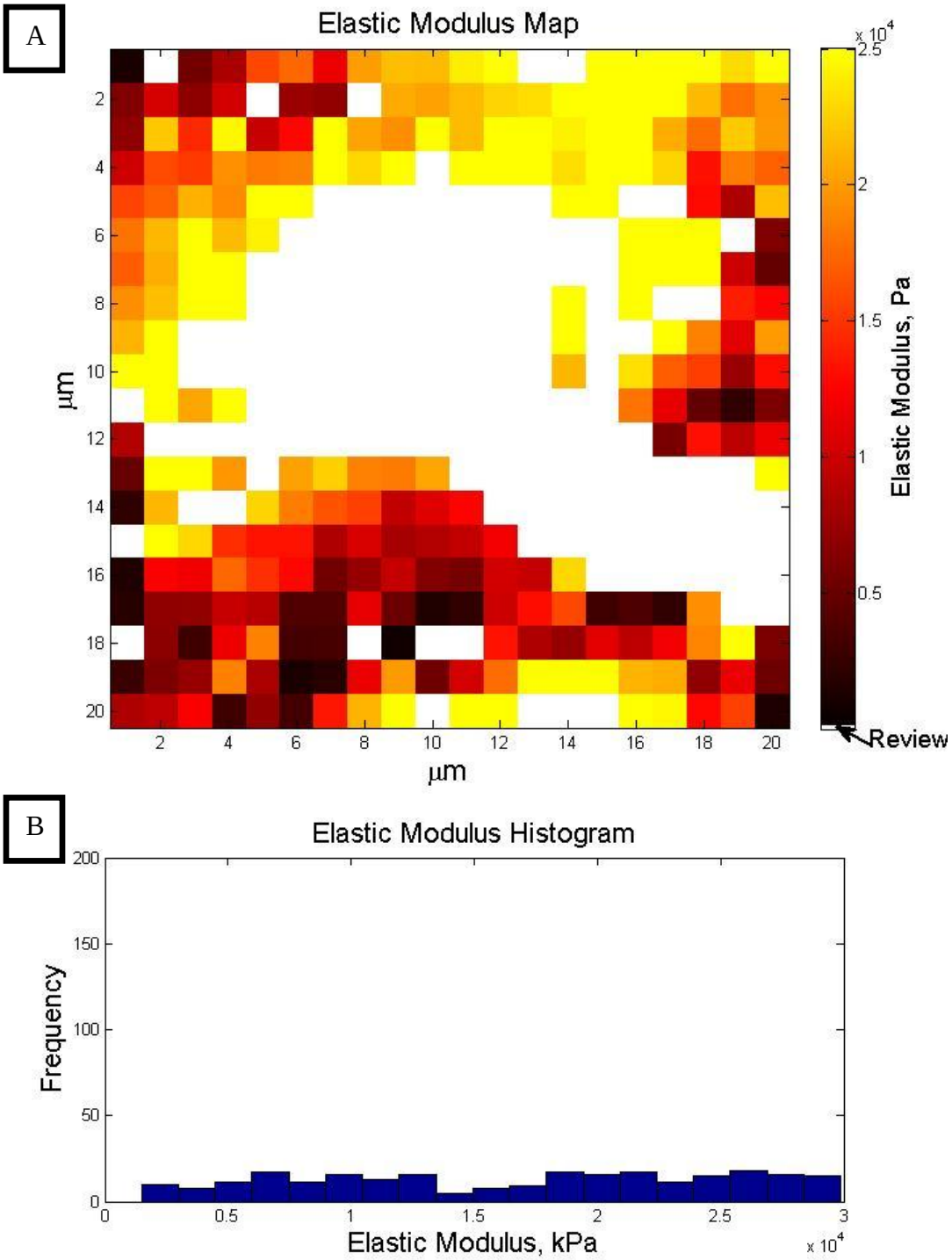

Figure 17. Iso6d3 Elastic Modulus Map and Histogram. The caption in Figure 16 represents the same information in this figure.

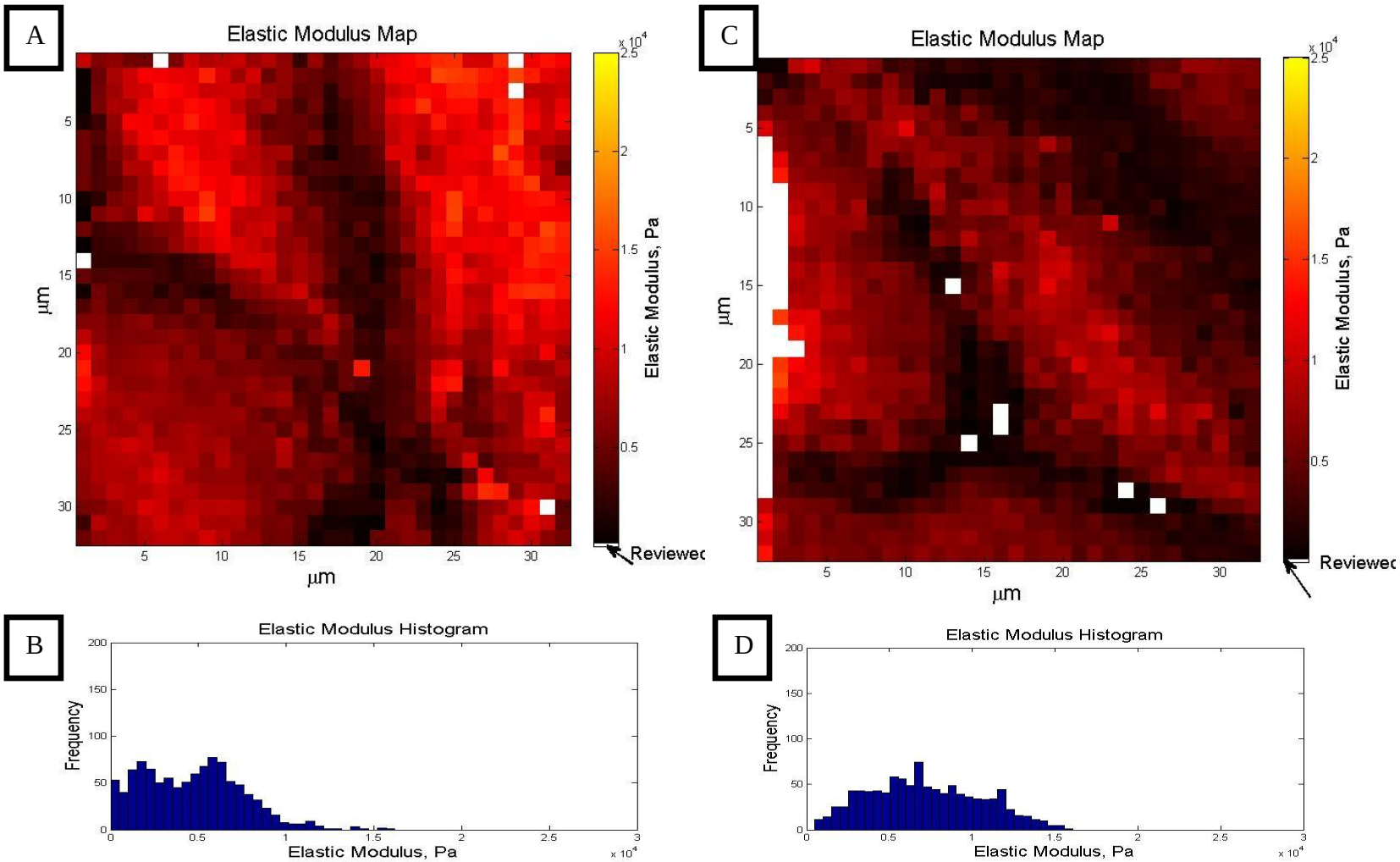
A
Elastic Modulus Map
µm
µm
x 10^4
Elastic Modulus, Pa
Reviewed
C
Elastic Modulus Map
µm
µm
x 10^4
Elastic Modulus, Pa
Reviewed
B
Elastic Modulus Histogram
Frequency
Elastic Modulus, Pa
x 10^4
D
Elastic Modulus Histogram
Frequency
Elastic Modulus, Pa
x 10^4

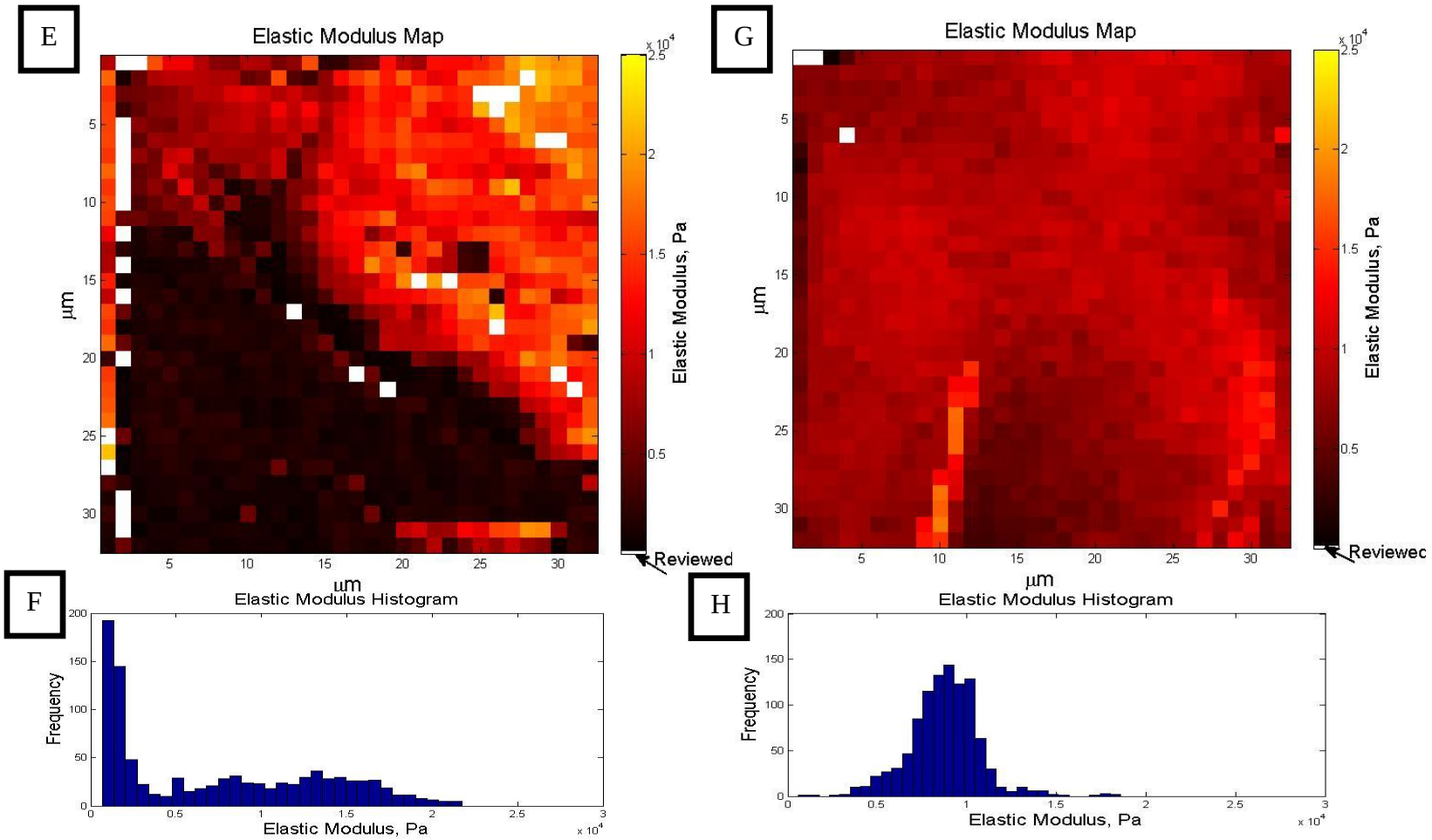

Figure 18. Iso7d2 (A, B, C, and D) and Iso7d3 (E. F. G, and H) Elastic Modulus Maps and Histograms. Each day had two maps produced on different sites. A, C, E, G relate to the elastic modulus maps and B, D, F, H relate to the histogram captions found in Figure 16

Table 4. *Average Elastic Modulus for Elastic Modulus Maps*.

	Average Elastic Modulus (kPa)	**Standard Deviation (kPa)**	**Accepted Curves**	**Accepted/Attempted Curves**
iso5d2	10.7	6.4	918	89%
iso6d3	14.3	7.8	264	66%
iso7d2 site1	7.3	3.4	1012	99%
iso7d2 site 2	4.9	2.7	971	95%
iso7d3 site 1	7.4	6.3	991	97%
iso7d3 site 2	8.7	1.9	1013	99%

Statistical Analysis

The elastic modulus means, medians, and acceptance rates for each isolation and day are illustrated in Figure 19. The mean differs from the median in isolations 1, 3-5, and 6. The mean tends to be similar to the median in isolations 2 and 7. The mean and median differences indicate that there data is not normally distributed. The acceptance percentage of curves tends to rise with the increased number of isolations. The median was a robust indicator of the elastic modulus and was used for calculation in Figure 20. Figure 20 shows a difference in days 2 ($n = 4570$) and 3 ($n = 5931$) the days were compared using the Mann-Whitney U test to determine if there was a significant difference. There was a significant difference at $\alpha = 0.05$. The p value was equal to or less than 0.001.

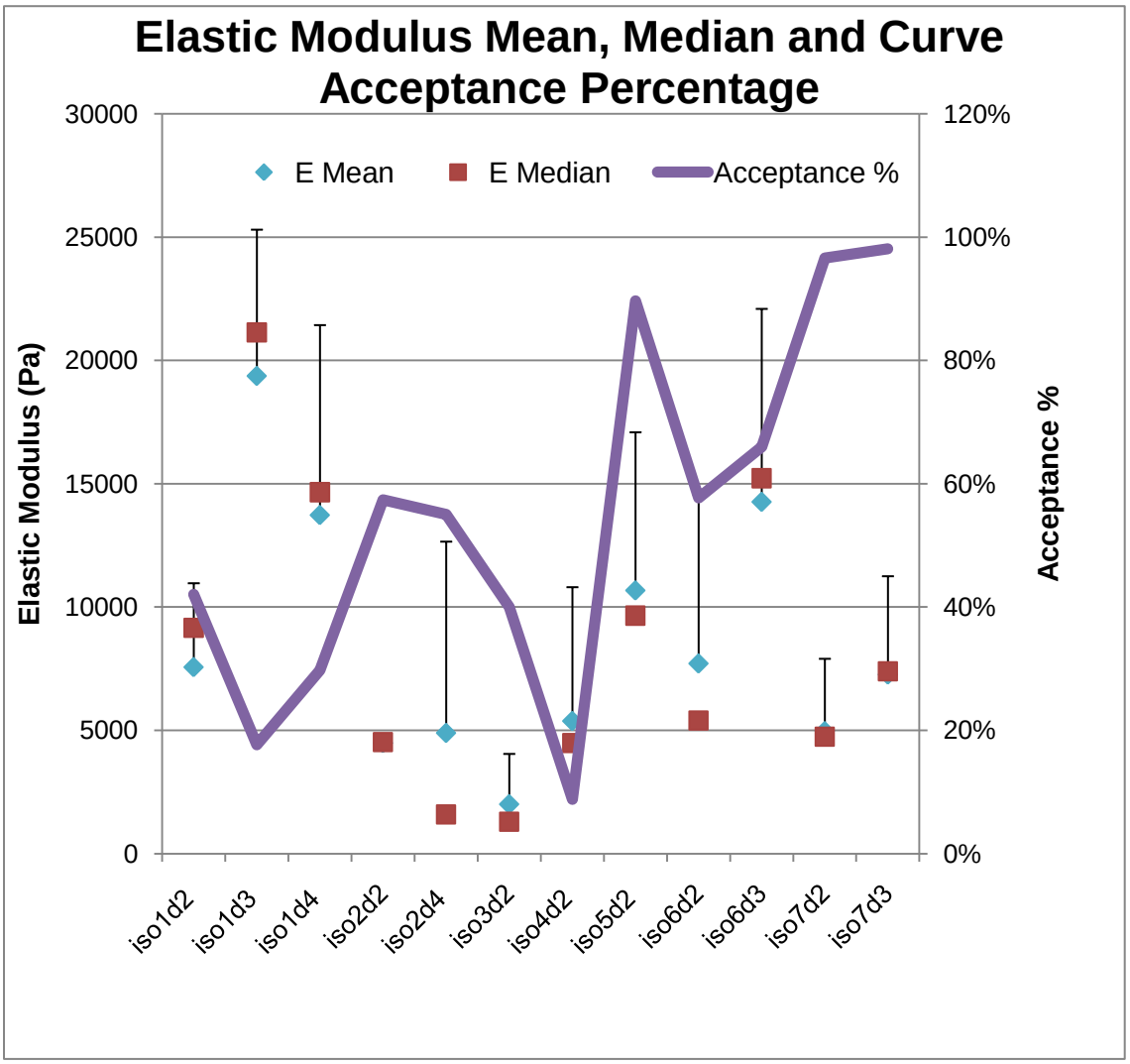

Figure 19. Median and Mean Elastic Modulus with Curve Acceptance Percentage. The primary vertical axis represents the elastic modulus (Pa), the secondary vertical axis represents the acceptance percentage (accepted/attempted curves X 100) and the horizontal axis represents the isolation and day. The error bars are standard deviation.

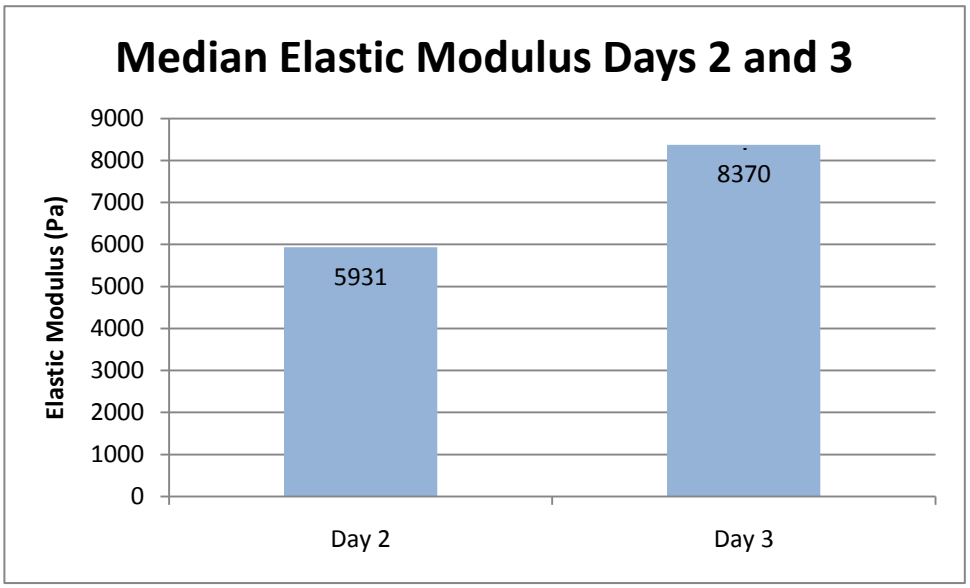

Figure 20. Median Elastic Modulus of Days 2 (n=4570) and 3 (n=5931), $p \leq 0.001$.

Chapter 5: Discussion

The data presented in the results chapter and the challenges to obtaining the results, e.g. the process for plating ATII cells, methods for calibration, F-δ, and imaging processes for data analysis, and statistical analysis are discussed.

Alveolar Epithelial Type II Cells

Plating

The plating of the ATII cells was successful. As noted in the results, the cell seeding density was near the expected level (93% of 3.5 X 10^6 cells/ml). The loss of cells could be related to the attachment of the cells to the inside walls of the pipette or the walls of the plastic screw topped test tube. The ATII cells were known to adhere to glass and plastic substrates.

Some isolations had incomplete or missing data because of difficulties with the cells becoming 100% confluent (Tables 2 and 3). This was common with primary cells because the isolation technique was not performed in a sterile hood. There were several points at which a pathogen could be introduced to the ATII cell culture. To the extent, it was possible to choose successfully plated cells in good condition, the AFM F-δ and imaging results represent the healthy, confluent ATII cells. Future studies could seed the primary ATII cells at a higher density or more plates of coverslips could be used to ensure that there are enough confluent coverslips for testing.

AFM Measurements

The AFM was a highly sensitive instrument, which needs to be calibrated regularly to perform F-δ and imaging properly. This section discusses the results of the AFM-related information.

AFM Calibration

The spring constant and the resonant frequency of the cantilever beam were determined each time a new cantilever was used on the ATII cells. The calibration process was deemed successful at determining the spring constant within the manufacturer's specifications for each isolation (Table 3).

AFM F-δ

The F-δ measurements were taken using two different software packages. The first package was a crude, user-defined package named Chad that was an add-on to the IGOR software. The Chad program did not allow the force measurements to take place until a topographical image of the region was complete, which was challenging. Having to complete the image before beginning F-δ measurements increased the time that the ATII cells were out of the incubator; therefore, fewer F-δ measurements could be performed on the cells before the cells were deemed non-viable (~2 hours outside of the incubator). The Chad program did not record which F-δ curves correlated with each topographical image of cells; therefore, showing a topographical image with the

corresponding force measurements was not possible. The second software package was part of an upgrade to IGOR; it allowed for F-δ measurements without a topographical image. By eliminating the topographical map, which took 35-40 minutes to complete, the time that would have been spent on the topographical map could be spent on F-δ measurements. The updated software package was able to save the force measurements in groups that corresponded to entire force maps (1024 curves per map).

Both software packages were able to produce F-δ curves that were suitable for analysis. The difficulty would lie in the variable height of the cell surface for the measurements. The AFM cantilever could be moved in the z-direction by a predetermined amount (calculated by an IGOR algorithm). If the cell height increased over a short horizontal distance more than the predetermined amount then the cantilever would run into the side of the cell between measurements instead of beginning a force measurement. Moving the cantilever horizontally into the ATII cell would cause a pre-contact force-distance curve where the true contact point was unknown and the model of mechanical events would not apply.

The velocity chosen for the cantilever to approach the ATII cell used was 1.03 μm/s. This value which was less than the values of 10 μm/s Azeloglu et al., (2008), and of 6 μm/s Alcaraz et al. (2003). It was similar to the value of 1.8 μm/s Rico et al., (2005). The elastic modulus reported in these papers decreased with the velocity of the cantilever in the z-axis decreasing. However, several factors were not identical: different mathematical models to extract the elastic modulus and two different cell types were

studied primary ATII cells and A549 cells (immortalized adenocarcinoma cells). A study of this variable is warranted.

The tips of the cantilevers were pyramidal shaped with blunt end radii, i.e., 10-40 nm. They were similar to those used by others (Alcaraz et al., 2003; Azeloglu, Bhattacharya, and Costa, 2008; Rico et al., 2005; Rico et al., 2005). The Sneddon adaptation accounts for the geometry of the tip and the contact surface area, but the indentation should remain small for optimal mechanics model validity. To avoid correcting the Hertz model to fit the cantilever, a cantilever with a spherical ball attached to the tip with a radius of 500 nm can be used. The spherical cantilever has a greater surface area to collect debris (dead cells, proteins etc) from the media and the debris would collect under the sphere before testing effect the results of the force measurements. If the materials collect under the cantilever, the measurements of the cells could be altered because the measurements would include the debris on the cantilever.

AFM Imaging

The topographical image created with the use of the AFM of ATII cells (Figure 14). Figure 14 shows a clear nuclear region of increased relative height and an area of cell edge. Figure 14 illustrates that the ATII cells were approximately 40μm wide. Also noted, were several small artifacts in the lower right hand corner of the map, these could be either lamellar bodies close to the surface of the cell or artifacts of the AFM topographical scan. Figure 14 shows the height of the ATII cell relative to the lowest area in the height map. This was not the absolute height of the ATII cell because at the

time that the image was produced the cells had grown to confluence, so there was no exposed part of the glass coverslip available to be imaged. The lowest portions of the topographical map were the lowest portions of the cells, not the glass coverslip, so no absolute height data can be concluded from the map.

Elastic Modulus Computation

The theory of extracting the elastic modulus from non-linear materials using indentation studies was well known (Hertz, 1882), but the steps and programs to minimize the solutions and find the correct elastic modulus were not widely discussed. The process of accepting good curves and rejecting poorly fit curves by some type of criteria was not examined in the literature.

The MATLAB program accepts files with the F-δ data from the IGOR software, spring constant values of the cantilevers based on user input, the equation (2); it uses the routine fminsearch to minimize solutions and find the correct elastic modulus solution. The program reviews or eliminates curves with poor fit using R^2, user generated maximum accepted elastic modulus, and user generated indentation depth.

The input variables of indentation depth and maximum accepted elastic modulus were varied to find the appropriate indentation that would yield the best curve fits to the data (Appendix A). The resulting indentation depth for the analysis was 300 nm because the depth was appropriately large enough to measure the mechanical properties of the whole cell. The indentation depth of 200 nm was thought to have been measuring events associated with the plasma membrane, not the entire cell (Leonenko et al., 2007). The

indentation of 500 nm results in too large of an indentation of the cell and could be subject to substrate affects. Substrate affects occur when the thickness of the cell in some regions was less than or equal to 500 nm, this also lead to poor curve fitting; therefore, many force measurements were eliminated based on low R^2 values. In Leonenko et al., the optimal indentation was 500 nm. There was a 10% decrease in the elastic modulus of ATII cells from 300 nm indentation to 500 nm of indentation due to cantilever beam geometry.

The indentation value should be small compared to the height of the cell when the Hertz model was used because the substrate mechanical characteristics could alter the elastic modulus results. Yet, the absolute height of the cell in each location of the force measurement was unknown. The relative height was known and inferences can be made about which area of the cell was taller than another can but the absolute height from the glass coverslip to the top of the cell was not known. The literature does not include cell height in the elastic modulus calculations.

When extracting E, the values of maximum accepted elastic modulus were varied between 30 kPa and 100kPa. The rationale for varying the maximum elastic modulus was to eliminate any elastic modulus that had substrate effects. The substrate effects were the result of the indentation depth not meeting the Hertz model assumption that the indentation must be small compared to the height. The edges of the cell could be thin and the indentation depth could be substantial in that area. This would result in an increased elastic modulus due to substrate effects. Therefore, a limit to the value of elastic modulus was varied. When the maximum elastic modulus was set at 100kPa, the results showed

that the standard deviation and the mean were oftentimes equal to each other or the standard deviation was greater than the mean. The elastic modulus did not have a normal distribution but a skewed distribution and thus traditional statistical testing would have had limited validity.

Mapping

The white pixels (Figures 16, 17, and 18) show which curves were eliminated from the analysis. This was not similar to literature where the poor fitting curves were not mentioned in print but only in personal conversations. These results show which force measurements have been eliminated. In addition, the results show the location relative to other force measurements. An important note, as the experience level of performing force indention measurements increased, the number of eliminated curves decreased.

In the elastic modulus maps, several distinct regions of high elastic modulus and low elastic modulus were visible (Figures 16, 17, and 18). The low elastic modulus regions tend to the values for elastic modulus found in the literature (Alcaraz et al., 2003; Azeloglu et al., 2008; Leonenko et al., 2007; Rico et al., 2005). These areas of low elastic modulus could relate to the nuclear region of the cell. The high elastic modulus regions could relate to the tight junctions between cells. The elastic modulus varies with the site on the map, the region of the plated cells, and the different number of cells covering the maps. The proportion of map coverage by the nuclear region or the cell edge or the cytoplasm also varies between maps. In the future, either the indentation

measurements can be coupled with optical images of the same region of the ATII cells with a fluorescent microscope mounted on the AFM or marking the location of the ATII cells in the elastic modulus map and fixing said cells to be stained for the nuclear region and optically imaged. These capabilities are commonly used outside of this research.

Statistical Analysis

The acceptance percentage in Figure 19 shows an increase over isolations 1-7, this was likely due to an increase in proficiency on the part of the researcher. This increase was due to learning the IGOR software and various intangibles of working with the AFM. Figure 19 shows a difference in the mean and median elastic modulus values for most isolations and days. The difference tends to show that the data was non-parametric in distribution. In isolation 7 which has the highest acceptance rate, the mean and median values tended to be similar. Since, the median values tended to be a more robust indicator of the data they were used in the non-parametric Mann-Whitney U test. The results showed $p \leq 0.001$, which was significant. This significant difference indicates that the mechanical properties of ATII cells exhibit a dependence on time.

More elastic modulus values from the day 2 data fell between 5-6 kPa. This differs compared to previously published studies where the range of values were from 1.4 ± 1.4 to 4.7 ± 2.9 kPa (Alcaraz et al., 2003; Azeloglu et al., 2008; Rico et al., 2005; Rico et al., 2005). This study falls more in line with the cytoplasmic measurements of the Azeloglu et al., (2008) study, although the study used neonatal primary rat ATII cells and the non-Hertzian method to compute the elastic modulus. The elastic modulus values

tend to be very similar on day 2. For future studies, the histograms could be analyzed to determine if the 5-6 kPa range exists on all day 2 data and if a shift occurs in subsequent days.

The number of independent samples for the Mann-Whitney test was large. Each single F-δ curve was an independent sample. The distance between each curve was one micrometer; this close spacing of measurements in an x-y grid may result in dependence between samples. The values of δ are set by the z_0 and z values and the deflection, d. Each of these components of δ could have a value or an error that is correlated with the value nearby. In the case of similar values, the measurement would be replicated; new independent would not be collected. In the case of related errors, there would not be a cancellation of random error; a systematic error would be included. These cases suggest that a careful consideration of errors and independence of the measurements be a part of future efforts.

In future studies, a patterned typed of elastic modulus map could be used to touch more ATII cells over a larger area which could result in a normal distribution of elastic modulus and a parametric statistical test could be performed to compare the data. The patterned type of testing would decrease the number of measurements per cell and the resolution of the elastic modulus map would decrease but the increase in cells measured would lead to more consistent elastic modulus measurements. To accompany the patterned measurements, spatial statistics could be used to incorporate the geographical relationship between elastic modulus values on a map. This method could detect any commonalities in elastic moduli over cells or groups of cells.

Chapter 6: Conclusions

The project hypothesizes was that the elastic modulus of ATII cells, measured with the use of an AFM in indentation mode, exhibit a dependence on time in culture. The methods were to grow primary alveolar epithelial type II cells to confluence for 48 hours; to produce a topographical image of living ATII cells using an AFM; to perform force spectroscopy measurements on confluent ATII cells; and to extract the elastic modulus using Hertzian mechanics from the force spectroscopy measurements. The conclusions of this work were:

1. The material characteristic of interest was the elastic modulus of ATII cells. To calculate the elastic modulus from indentation information requires the use of the Hertz-Sneddon or another indentation model. The F-δ curves were analyzed using fminsearch, a least squares non-linear regression, to find the line of best fit using the Hertz-Sneddon indentation equation model to calculate the elastic modulus of the ATII cells from the F-δ curves. The resulting elastic moduli were mapped by the original location of the measurement. The mapping showed a grouping of areas of high and areas of low elastic modulus.

2. The statistical analysis of the median value of the elastic modulus showed a significant difference between days 2 and 3. An increase was observed in elastic modulus was observed.

The specific aims to obtain a conclusive result to accept or reject the hypothesis were completed. The elastic modulus for each isolation and day did show a significant increase over the days 2 and 3. The elastic modulus maps also showed regions of high and low elastic modulus that could correlate with the ATII cell's morphology. The topographical image of the ATII cells shows the size and relative height of the cells.

Chapter 7: Future Work

Future work to study the elastic modulus during the differentiation of alveolar epithelial type II cells using the atomic force microscope to perform indentation force measurements should include:

i. Optical Images: A fluorescent microscope could be mounted to the AFM to produce live images of the ATII cells that undergoing force measurements. This would provide information about the nuclear region relative to the elastic modulus regions.

ii. Velocity of Cantilever Study: The velocity of the cantilever when approaching the ATII cells differs greatly in the literature and a study examining the velocity and the relation to elastic modulus would fill a literature gap.

iii. Cell Height Information: The cell height information was needed to implement corrections to the Hertz model. If possible, the cell height at the location of each force measurement could be calculated then the indentation depth could be adjusted to be small in comparison to the height of the cell in that location.

iv. Spherical Cantilever: The spherical cantilever would also need to be used to implement the Hertz model. The sphere should be 1 μm or greater to have an indentation value of 500 nm.

v. Patterned Force Indentation Maps: Create a patterned F-δ map to cover a greater area of the cells; therefore, increasing the number of cells touched.

The test of the hypothesis showed a significant difference in days 2 and 3. The work here provides basic elements of an approach for the future testing of this hypothesis. The future work suggestions could result in new learning about the ATII cells mechanical characteristics.

Bibliography

Adams, G. G., & Nosonovsky, M. (2000). Contact Modeling- Forces. *Tribology International*, 431-442.

A-Hassan, E., Heinz, W. F., Antonik, M. D., D'Costa, N. P., Nageswaran, S., Schoenenberger, C.-A. et al. (1998). Relative microelastic mapping of living cells by atomic force microscopy. *Biophysical Journal*, 1564-1578.

Alcaraz, J., Buscemi, L., Grabulosa, M., Trepat, X., Fabry, B., Farre, R. et al. (2003). Microrheology of human lunch epitheial cells measured by atomic force micorscopy. *Biophysical Journal*, 2071-2079.

Alenghat, F. J., Fabry, B., Tsai, K. Y., Goldmann, W. H., & Ingber, D. E. (2002). Analysis of Cell Mechanics in Single Vinculin-Deficient Cells Using a Magnetic Tweezer. *Biochemical & Biophysical Research Communications*, 93-99.

Ashino, Y., Ying, X., Dobbs, L., & Bhattacharya, J. (2000). [Ca2+]i oscillations regulate type II cell exocytosis in the pulmonary alveolus. *Am J Physiol Lung Cell Mol Physiol*, 5-13.

Ashkin, A., Dziedzic, J. M., Bjorkholm, J. E., & Chu, S. (1986). Observation of a single-beam gradient force optical trap for dielectric particles. *Opt Lett*, 288-290.

Azeloglu, E., Bhattacharya, J., & Costa, K. (2008). Atomic force microscope elastography reveals phenotypic difference in alveolar cell stiffness. *Journal of Applied Physiology*, 652-661.

Barrett, K. E., Barman, S. M., Boitano, S., & Brooks, H. L. (2010). Mechanics of Respiration. In K. E. Barrett, S. M. Barman, S. Boitano, & H. L. Brooks, *Ganong's Review of Medical Physiology, 23e.* United States: McGraw-Hill.

Bausch, A. R., Moller, W., & Sackmann, E. (1999). Measurement of Local Viscoelasticity & forces in living cells by magnetic tweezers. *Biophyical Journal*, 573-579.

Berdyyeva, T. K., Woodworth, C. D., & Sokolov, I. (2005). Human Epithelial cells increase their rigidty with ageing invitro: direct measurements. *Phys Med Biol*, 81-92.

Berrios, J. C., Schroeder, M. A., & Hubmayr, R. D. (2001). Mechanical properties of alveolar epithelial cells in culture. *Journal of Applied Physiology*, 65-73.

Berthiaume, Y. (1999). Treatment of adult respiratory distress syndrome: plea for rescue therapy of the alveolar epithelium. *Quality & Safety in Health Care*, 150.

Boitano, S., Safdar, Z., DG Welsh, J. B., & Koval, M. (2004). Cell-cell interactions in regulatin lung function. *Am J Physiol Lung Cell Mol Physiol*, 65-73.

Charras, G., Lehenkari, P., & Horton, M. (2001). Atomic force microscopy can be used to mechanically stimulate osteoblasts & evaluate cellular strain distributions. *Ultramicroscopy*, 85-95.

Cheek, J., Evans, M., & Cr&al, E. (1989). Type I cell-like morphology in tight alveolar epithelial monolayers. *Exp Cell Res*, 375-87.

Costa, K. D. (2003, 2004). Single-cell Elastography: Probing for disease with the Atomic Force Microscope. *Disease Markers 19*, 139-154.

Costa, K. D., Hucker, W. J., & Yin, F. C. (2002). Buckling of Actin Stress Fibers: A New Wrinkle in the Cytoskeletal Tapestry. *Cell Motil Cytoskelelton*, 266-274.

Costa, K., Sim, A., & Yin, F. (2006). Non-Hertzian approach to analyzing mechanical properties of endothelial cells probed by atomic force microscopy. *J Biomechanics*, 176-184.

Dailey, H. L., Ricles, L. M., Yalcin, H. C., & Ghadiali, S. N. (2009). Image baded inite element modeling of alveolar epithelial injury during airway opening. *J Appl Physiol*, 221-232.

Dailey, H. L., Yalicin, H. C., & Ghadiali, S. N. (2007). Fluid-structure modeling of flow induced alveolar epithelial cell deformation. *Computers & Structures*, 1066-1071.

Desai, L., Sinclair, S., Chapman, K., Hassid, A., & Waters, C. (2007). High tidal volume mechanical ventilation with hyperoxia alters focal adhesions of alveolar type II cells. *Am. J. Physiol. Lung Cell. Mol. Physiol.*, L769-L778.

Dimitriadis, E., Horkay, F., Maresca, J., Kachar, B., & Chadwick, R. S. (2002). Determination of elastic moduli of thin layers of soft material using the Atomic Force Microscope. *Biophysical Journal*, 2798-2810.

Dobbs, L. G., Williams, M. C., & Br&t, A. E. (1985). Changes in biochemical characteristics & pattern of lectin binding of alveolar type II cells with time in

culture. *Biochimica et Biophysica Acta (BBA) - Molecular Cell Research*, 155-166.

Dobbs, L. (1990). Isolation & culture of alveolar type II cells. *American Journal of Physiology*, 134-147.

Dobbs, L., Gonzalez, R., & Williams, M. (1986). An improved method for isolating type II cells in high yield & purity. *Am Rev Respir Dis*, 141-145.

Dublin, K., Mager, E., Allen, L., Tigue, Z., Goodglick, L., Wadehra, M. et al. (2004). Identification of gene differentially expressed in rat alveolar type I cells. *Am J Respier Cell Mol Biol*, 309-316.

Ehrhardt, C., Kim, K.-J., & Lehr, C.-M. (2005). Isolation & Culture of Human Alveolar Epithelial Cells. In *Methods in Molecular Medicine* (pp. 207-216). Humana Press.

Fehrenbach, H. (2001). Alveolar epithelial cell type II: defender of the alveolus revisted. *Resp Research*, 33-46.

Fels, A. O., & Cohn, Z. A. (1986). The alveolar macrophage. *Journal of Applied Physiology*, 353-369.

Fereol, S., Fodil, R., Pelle, G., Louis, B., & Isabey, D. (2008). Cell mechanics of alveolar epithelials cells & macrophages. *Resp Physiol & Neurbiol*, 3-16.

Fick's Law of Diffusion. (2010). Retrieved February 28, 2010, from Encyclopedia Btriannica: http://www.britannica.com/EBchecked/topic/206032/Ficks-law-of-diffusion

Fminsearch MATLAB Function Reference. (2010). Retrieved March 15, 2010, from Mathworks: http://www.mathworks.com/access/helpdesk_r13/help/techdoc/ref/fminsearch.html

Fournier, M. F., Sauser, R., Ambrosi, D., Meister, J.-J., & Verkhovsky, A. B. (2010). Force Transmission in migrating cells. *J of Cell Biology*, 287-297.

Fuchs, S., Hollins, A. J., Laue, M., Schaefer, U. F., Roemer, K., Gumbleton, M. et al. (2003). Differentiation of human alveolar epithelial cells in primary culture: morphological characteriztion & synthesis of caveolin-1 ans surfactant protein-C. *Cell Tissue Res*, 31-45.

Griese, M. (1999). Pulmonary surfactant in health & human lung diseases:. *Eur Respir*, 1455-1476.

Gutierrez, J., Gonzalez, R., & Dobbs, L. (1998). Mechanical distension modulates pulmonary alveolar epithelial phenotypic expression in vitro. *Am J Physiol*, L196-202.

Heidemann, S. R., Kaech, S., Buxbaum, R. E., & Matus, A. (1999). Direct Observations of the Mechanical Behaviors of the Cytoskeleton in Living Fibroblasts. *J. Cell Biol*, 109-122.

Hertz, H. (1896). *Miscellaneous Papers* . London: Macmillan.

Hertz, H. (1882). Uber die beruhrung fester elastischer Kroper. *J Reine Angew*, 156-171.

Hochmuth, R. M. (2000). Micropipette aspiration of living cells. *J of Biomechanics*, 15-22.

Holzapfel, G. A., & Ogden, R. W. (2006). *Mechanics of Biological Tissue.* Springer.

Ingber, D. (1997). Tensegrity: the architectural basis of cellular mechanotransduction. *Annu Rev Physiol*, 575-599.

Kobayashi, S., Kondo, S., & Juni, K. (1995). Permeability of Peptides & Proteins in Human Cultured Alveolar A549 Cell Monolayer. *Pharmaceutical Research*, 1115-1119.

Lagarias, J., Reeds, J. A., Wright, M. H., & Wright, P. E. (1998). Convergence Properties of the Nelder-Mead Simplex Method in Low Dimensions. *SIAM Journal of Optimization*, 112-147.

Laurent, V. M., Henon, S., Planus, E., Fodil, R., Ball&, M., Isbey, D. et al. (2002). Assesment of mechanical proerpties of adherent living cells by bead micromanipulation: comparison of magnetic twisting cytometry vs optical tweezers. *Journal of Biomedical Engineering*, 408-421.

Leonenko, Z., Finot, E., & Amrein, M. (2007). Adhesive interaction measured between AM probe & lung epithelial type II cels. *Ultramicroscopy*, 948-953.

Lin, D., Dimitriadis, E. K., & Horkay, F. (2007a). Robust Strategies for automated AFM curve analysis--II: Adhesion-influenced indentation of soft, elastic materials. *Journal of Biomedical Engineering*, 904-912.

Lin, D., Dimitriadis, E., & Horkay, F. (2007b). Robust strategeies for automated AFM curve analysis--I: Non-adhesive indentation of soft inhomogeneous materials. *Journal of Biomedical engineering*, 430-440.

Lou, H. X., & Yu, L. (1999). Atomic force microscopy imaging of living cells: progress, problems & prospects. *Methods in Cell Science*, 1-17.

Luis M. Argote-Greene, M. Y. (2005). Extrapleural pneumonectomy for malignant pleural mesothelioma. *Multimedia Manual of Cardiothoratic Surgery* .

Maniotis, A. J., Chen, C. S., & Ingber, D. E. (1997). Demonstration of Mechanical Connections Between Integrins, Cytoskeletal Filaments, & Nucleoplasm that Stabilize Nuclear Structure. *Proc. Natl. Acad. Sci.*, 849-854.

Nelder, J. A., & Mead, R. (1965). A simplex method for function minimization. *Computer Journal*, 308-313.

Ochs, M., Nyengaard, J. R., Jung, A., Knudsen, L., Voigt, M., Wahlers, T. et al. (2004). The Number of Alveoli in the Human Lung. *American Journal of Respiratory & Critical Care Medicine*, 120-124.

Oekler, R., & Hubmayr, R. D. (2008). Cell Wounding & repair in ventiliator injured lungs. *Resp Physiol & Neurobiol*, 44-53.

Ohayon, J., Tracqui, P., Rodil, R., Fereol, S., Planus, E., & Isabey, D. (2004). Analysis of nonlinear responses of adherent epithelial cells probed by a magnetic bead twisting: a finite element model based on a homogenization approach. *J of Biomechanics Engineering*, 685-698.

Olsen, C. E., Isakson, B. E., Seedorf, G. J., Lubman, R. L., & Boitano, S. (2005). Extracellular matrix-driven alveolar epithelial cell differentiation in vitro. *Exp Lung Research*, 461-482.

Pavelka, M., & Roth, J. (2005). *Functional Ultrastructure An Atlas of Tissue Biology & pathology.* Austria: Springer Verlag/Wein.

Radmacher, M. (1997). Measuring the elastic properties of biological samples with the AFM. *IEEE Eng. Med. Biol. Mag.*, 47-57.

Radmacher, M. (2007). Studying the Mechanics of Cellular Processes by Atomic Force Microscopy. *Methods in Cell Biology*, 347-372.

Ratner, B. D. (2004). *Biomaterials Science: An Introduction to Materials in Medicine.* Academic Press; 2nd edition.

Rico, F., Alcaraz, J., Fredberg, J. F., & Navajas, D. (2005). Nanomechanics of lung epithelial cells. *Int J Nanotechnology*, 180-194.

Rico, F., Roca-Cusachs, P., Gavara, N., Farré, R., Rotger, M., & Navajas, D. (2005). Probing mechanical properties of living cells by atomic force microscopy with blunted pyramidal cantilever tips. *Phys. Rev. E*, 1-10.

Sahinidis, N. V. (2010, March 16). Derivative-free optimization: A review of algorithms & comparison of software implementations. 1-54. (A. Cozad, Interviewer)

Seo, Y., & Jhe, W. (2008). Atomic Force Microscopy & Spectroscopy. *Reports on Progress in Physics*, 1-23.

Sinclair, S., Molthen, R., Hayworth, S., Dawson, C., & Waters, C. (2007). Airways strain during mechanical ventilation in an intact animal model. *Am J. Resp. Crit. Care Med.*, 786-794.

Sneddon, I. N. (1965). The relation between load & penetration in the axisymmetric boussinesqu problem for a punch of arbitrary profile. *Int J of Engineering Science*, 47-57.

Stroetz, R. W., Vlahakis, N. E., Walters, B. J., Schroeder, M. A., & Hubmayr, R. D. (2001). Validation of new live cells strain system: characterization of plasma memeber stress failure. *J Appl Physiol*, 2361-2370.

Sugahara, K., Tokumine, J., Teruya, K., & Oshiro, T. (2006). Alveolar epithelial cells: differentiation & lung injury. *Respirology*, S28 - S31.

Sugawara, M., Ishida, Y., & Wada, H. (2004). Mechanical properties of sensory & supporting cells in the organ of Corti of the guinea pig cochlea - study by atomic force microscope. *Hearing Research*, 57-64.

Suki, B., Ito, S., Stamenovic, D., Lutchen, K. R., & Ingenito, E. P. (2005). Biomechanics of the lung parenchyma: critical roles of collagen & mechanical forces. *J Appl Physiol*, 1892-1899.

Sultan, C., Stamenovic, D., & Ingber, D. E. (2004). A Computational Tensegrity Model Predicts Dynamic Rheological Behaviors in Living Cells. *Ann of Biomedical Engineering*, 52-530.

Thoumine, O., Ott, A., Cardoso, O., & Meister, J. (1999). Microplates: a new tool for manipulation of indivdual cells. *J Biochem Biophys Methods*, 47-62.

Trepat, X., Grabulosa, M., Puig, F., Maksym, G. N., Navajas, D., & Farre, R. (2004). Viscoelasticity of Human Alveolar Epithelial Cells Subjected to Stretch. *Am J Physiol Lung Cell Mol Physiol*, L1025-L1034.

Van Golde, L., Batenburg, J., & Robertson, B. (1994). The pulmonary surfactant system. *News in Physiol Sciences*, 13-20.

Wagh, A. A., Roan, E., Chapman, K. E., Desai, L. P., Rendon, D. A., Eckstein, E. C. et al. (2008). Localized elasticity measured in epithelial cells migrating at a wound edge using atomic force microscopy. *Am J Physiol Lung Cell Mol Physiol*, L54–L60.

Wang, D., Havil D., Burns, A., & Sigmond, E. (2007). A pure population of lung alveolar epithelial type II cells derived from human embryonic stem cells. *Proc Natl Acad Sci USA*, 4449-54.

Wang, N., Bulter, J., & Ingber, D. (1993). Mechanotransduction across the cell surface & through the cytoskeleton. *Science*, 1124-1127.

Wei, M., Zaorski, A., Yalcin, H. C., Wang, J., Hallow, M., Ghaiali, S. N. et al. (2008). A comparative study of living cell micromechanical properties by oscillatory optical tweezers. *Optics Express*, 8594-8603.

Widwaimer, E., Raff, H., & Strang, K. (2003). *V&er, Sherman, Luciano's Human Physiology: The Mechanisms of Body Function.* McGraw-Hill (Tx).

Xuemei, S., Huilan, Z., Shengdao, X., Guohua, Z., Weining, X., Zhenxiang, Z. et al. (2007). Primary culture of alveolar epithelial type II cells & its bionomic study. *Journal of Huazhong University of Science & Technology -- Medical Sciences* --, 653-656.

Yeung, T., Georges, P. C., Flanagan, L. A., Marg, B., Ortiz, M., Funaki, M. et al. (2004). Effects of Substrate Siffness on Cell Morphology, Cytoskeletal Structure, & Adhesion. *Cell Motility & the Cytoskeleton*, 24-34.

Zhang, G., Long, M., Wu, Z., & Yu, W. Q. (2002). Mechanical properties of hepatocellular carcinoma cells. *World Journal of Gastroenterology*, 243-246.

Appendix

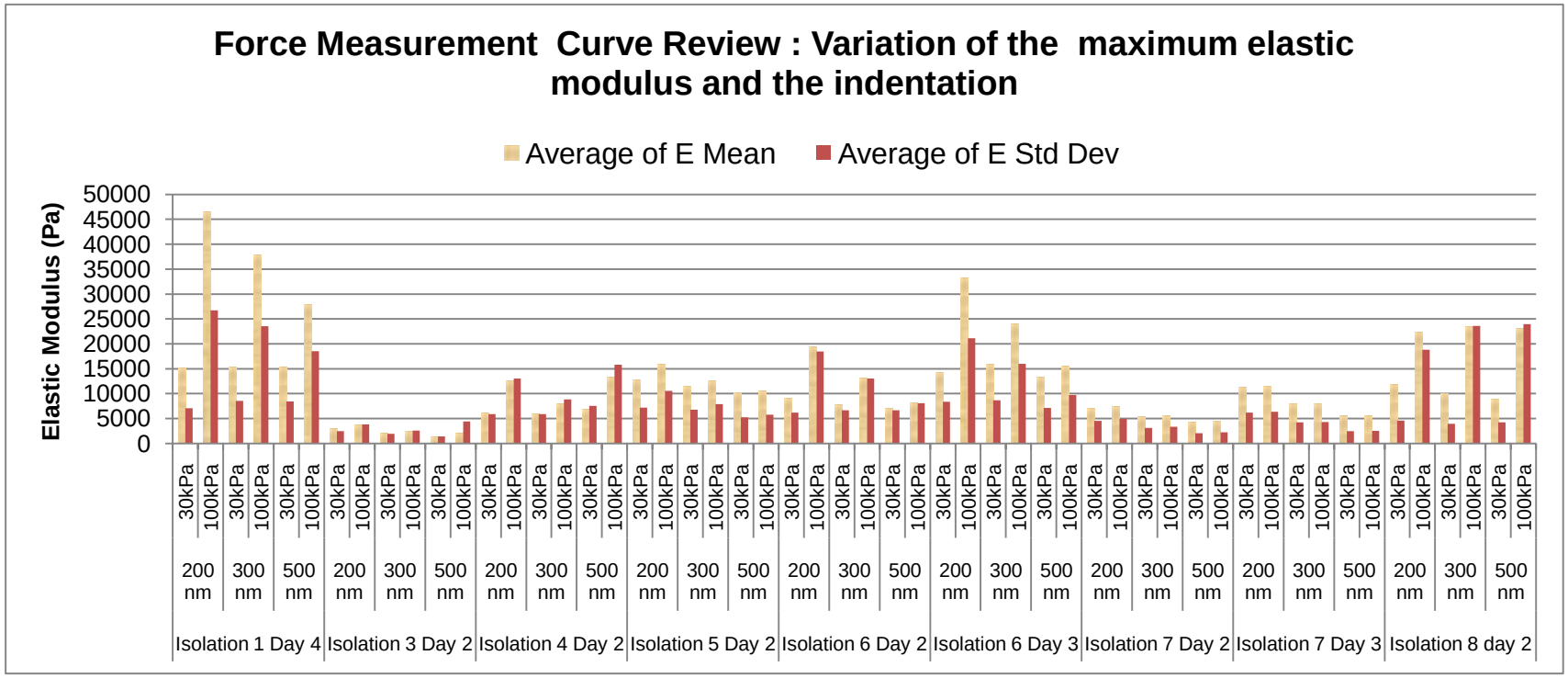

Figure 21: Force Measurement Curve Review. The indentation depth (200, 300, and 500 nm) and maximum accepted elastic modulus (30 kPa and 100 kPa) were varied for each set of data (isolation and day). The results show the mean and standard deviation of the elastic modulus.